Mon. Not. R. Astron. Soc. **000**, 000–000 (0000) Printed September 14, 2015 (MN LATEX style file v2.2)

The inferred evolution of the cold gas properties of CANDELS galaxies at $0.5 < z < 3.0$

G. Popping[1,2⋆], K. I. Caputi[2], S. C. Trager[2], R. S. Somerville[3], A. Dekel[4], S. A. Kassin[5], D. D. Kocevski[6], A. M. Koekemoer[5], S.M. Faber[7], H. C. Ferguson[5], A. Galametz[8], N. A. Grogin[5], Y. Guo[9], Y. Lu[10], A. van der Wel[11], and B. J. Weiner[12]

[1] *European Southern Observatory, Karl-Schwarzschild-Strasse 2, 85748, Garching, Germany*
[2] *Kapteyn Astronomical Institute, University of Groningen, Postbus 800, NL-9700 AV Groningen, the Netherlands*
[3] *Department of Physics and Astronomy, Rutgers University, 136 Frelinghuysen Road, Piscataway, NJ 08854, USA*
[4] *Racah Institute of Physics, The Hebrew University, Jerusalem 91904, Israel*
[5] *Space Telescope Science Institute, 3700 San Martin Drive, Baltimore, MD 21218, USA*
[6] *Department of Physics and Astronomy, University of Kentucky, Lexington, KY 40506, USA*
[7] *UCO/Lick Observatory, Department of Astronomy and Astrophysics, University of California, Santa Cruz, CA 95064, USA*
[8] *Max-Planck-Institut für Extraterrestrische Physik, Giessenbachstrasse, D-85748 Garching, Germany*
[9] *UCO/Lick Observatory, Department of Astronomy and Astrophysics, University of California, Santa Cruz, CA 95064, USA*
[10] *The Carnegie Observatories, Pasadena, CA 91101, USA*
[11] *Max-Planck Institut für Astronomie, Königstuhl 17, D- 69117, Heidelberg, Germany*
[12] *Steward Observatory, 933 N. Cherry St., University of Arizona, Tucson, AZ 85721*

September 14, 2015

ABSTRACT

We derive the total cold gas, atomic hydrogen, and molecular gas masses of approximately 24 000 galaxies covering four decades in stellar mass at redshifts $0.5 < z < 3.0$, taken from the CANDELS survey. Our inferences are based on the inversion of a molecular hydrogen based star formation law, coupled with a prescription to separate atomic and molecular gas. We find that: 1) there is an increasing trend between the inferred cold gas (H I and H_2), H I, and H_2 mass and the stellar mass of galaxies down to stellar masses of $10^8\,M_\odot$ already in place at $z = 3$; 2) the molecular fractions of cold gas increase with increasing stellar mass and look-back time; 3) there is hardly any evolution in the mean H I content of galaxies at fixed stellar mass; 4) the cold gas fraction and relative amount of molecular hydrogen in galaxies decrease at a relatively constant rate with time, independent of stellar mass; 5) there is a large population of low-stellar mass galaxies dominated by atomic gas. These galaxies are very gas rich, but only a minor fraction of their gas is molecular; 6) the ratio between star-formation rate (SFR) and inferred total cold gas mass (H I + H_2) of galaxies (i.e., star-formation efficiency; SFE) increases with star-formation at fixed stellar masses. Due to its simplicity, the presented approach is valuable to assess the impact of selection biases on small samples of directly-observed gas masses and to extend scaling relations down to tellar mass ranges and redshifts that are currently difficult to probe with direct measurements of gas content.

Key words: galaxies: evolution - galaxies: formation - galaxies: ISM - ISM: molecules

1 INTRODUCTION

Observations in the local Universe have revealed that star formation (SF) is closely linked to the density of molecular gas. SF in the Milky Way takes place in dense, massive and cold giant molecular clouds (Solomon et al. 1987; McKee & Ostriker 2007; Bolatto et al. 2008). Recent works have emphasized that there is a strong correlation between the star-formation rate (SFR) density and the density of molecular hydrogen (H_2), while the correlation with the density of atomic hydrogen (H I) is weak or absent (Wong & Blitz 2002; Bigiel et al. 2008, 2011; Schruba et al. 2011). These results have stimulated the idea that not all the cold gas in a galaxy is necessarily available for SF. A proper understanding of the evolution of the atomic and molecular gas

⋆ E-mail: gpopping@eso.org

content of galaxies is a key ingredient that will shed light on the physics that regulates the stellar buildup of galaxies.

Current surveys of the cold gas content of galaxies at high redshift only probe the molecular gas mass and are usually limited to massive galaxies with high SFR (e.g., Daddi et al. 2010; Tacconi et al. 2010; Geach et al. 2011; Bauermeister et al. 2013; Tacconi et al. 2013; Santini et al. 2013). It is crucial to include the contribution from atomic hydrogen to thoroughly understand how the total cold gas properties of galaxies regulate the SFR. Furthermore, for a complete assessment it is necessary to study a galaxy sample that is not biased to the most actively star-forming objects. It is hoped that facilities such as ALMA (Atacama Large Millimeter Array), NOEMA (NOrthern Extended Millimeter Array), SKA (Square Kilometer Array), MeerKat (Karoo Array Telescope) and ASKAP (Australian SKA Pathfinder) will reveal the H I and H_2 content of representative samples of high-redshift galaxies.

Theorists have made considerable progress developing models that track the H I and H_2 content of galaxies (Obreschkow & Rawlings 2009; Fu et al. 2010; Krumholz & Dekel 2012a; Lagos et al. 2011; Christensen et al. 2012; Kuhlen et al. 2012; Davé et al. 2013; Popping, Somerville & Trager 2014; Somerville, Popping & Trager 2015). These models have proven successful at reproducing the available observational estimates of the overall H I and H_2 properties of local and high-redshift galaxies. Nevertheless, observational constraints at high redshift are still very limited and do not probe the wide parameter space covered by the models. Additional information on the gas content of galaxies will be crucial to break the degeneracies in different physical mechanisms that are included in models (e.g., SF and stellar feedback).

In the meantime, we can obtain indirect constraints on the gas content of galaxies by using the empirical relation between SFR density and gas density. This approach has been used extensively by inverting the Schmidt-Kennicutt relation (Kennicutt 1998b, hereafter the KS-relation), which relates the SFR surface density to the combined atomic and molecular hydrogen surface density (e.g., Erb et al. 2006; Mannucci et al. 2009; Troncoso et al. 2013). Popping et al. (2012) were the first to use an inverted molecular-gas-based SF law in combination with a recipe to separate atomic from molecular hydrogen (Blitz & Rosolowsky 2006) to estimate the total cold gas and molecular gas content of galaxies. This approach was motivated by observations demonstrating that SFR surface densities correlate almost linearly with molecular gas surface density (even in the low gas surface density regime), whereas the KS-relation breaks down at low 'total gas' surface densities (Bigiel et al. 2008; Schruba et al. 2011). Popping et al. (2012) showed that, when inferring gas masses, a molecular-gas-based SF law in combination with a prescription to separate the atomic and molecular hydrogen content of galaxies is better suited to reproduce directly-observed gas masses and gas surface densities from a sample of galaxies taken from Leroy et al. (2008) than the total-gas KS-relation.

Popping et al. (2012) confirmed previously observed trends between galaxy gas fraction and molecular gas fraction with stellar mass (e.g. Tacconi et al. 2010; Saintonge et al. 2011), through a detailed study of the inferred gas content of galaxies in COSMOS (the Cosmic Evolution Survey Scoville et al. 2007) at $0.5 < z < 2.0$. This initial study suggested that massive galaxies have lower gas fractions at higher redshift than less-massive objects and have lower fractions of their gas in molecular form.

In this paper, we apply the method developed in Popping et al. (2012) and updated in Popping, Behroozi & Peeples (2015) to a galaxy sample drawn from the CANDELS survey (Cosmic Assembly Near-infrared Deep Extragalactic Legacy Survey; Grogin et al. 2011; Koekemoer et al. 2011) at redshifts $0.5 < z < 3$. We focus on the cold gas (H I + H_2), H I, and H_2 properties of galaxies over cosmic time and how they are related to the SF and other global properties of galaxies. The CANDELS survey is deeper than the COSMOS survey, which allows us to study much fainter objects. As such, we can probe the gas properties of the bulk of star-forming galaxies between $z = 0.5$ and $z = 3$. This cosmic epoch marks the peak in star-formation activity of our Universe (Hopkins & Beacom 2006; Madau & Dickinson 2014), when the bulk of mass in today's massive galaxies was formed. CANDELS provides exquisite imaging covering a wide range of wavelengths to derive stellar masses and SFR and provides reliable morphological information at these redshifts. The methodology enables us to infer the gas, H I, and H_2 masses for a large number of galaxies covering a wide range in stellar masses, SFRs, sizes, and redshift. This makes the applied method very helpful in assessing the impact of selection biases on much smaller samples for which direct gas measurements have been obtained. Furthermore, it can extend scaling relations to a stellar mass and redshift range difficult to reach through direct observations of gas masses. The inferred gas masses presented in this work have a great predictive power for future H I surveys such as LADUMA (Holwerda, Blyth & Baker 2012) with instruments like MeerKat, ASKAP, and the SKA and future surveys of the molecular hydrogen content of galaxies through CO or sub-mm continuum imaging with for example ALMA and NOEMA.

This paper is organised as follows. In Section 2 we summarise our method to indirectly measure the cold gas and H_2 content of galaxies and we present the galaxy sample selection from CANDELS. In Section 3 we present our results. The assumptions that were made and the applicability of our model to the CANDELS galaxy sample are discussed in Section 4. We discuss our results in Section 5. We summarise our findings in Section 6. Throughout the paper, we assume a Λ Cold Dark Matter (ΛCDM) cosmology with $H_0 = 70\,\mathrm{km\,s^{-1}\,Mpc^{-1}}$, $\Omega_{\mathrm{matter}} = 0.28$ and $\Omega_\Lambda = 0.72$ (Komatsu et al. 2009). We assume a universal Chabrier stellar initial mass function (IMF: Chabrier 2003) and where necessary convert observational quantities used to a Chabrier IMF. All reported cold, H I, and molecular gas masses include a correction of 1.36 to account for helium.

2 MODEL & DATA

In this section we describe our method to indirectly estimate the cold gas (H I +H_2), H I, and H_2 content of galaxies and the observational data to which we apply our method.

2.1 Obtaining indirect gas measures

We infer the cold gas (H I + H_2), H I and H_2 content of galaxies using a combination of an empirical molecular SF law (based on Bigiel et al. 2008) and a prescription to calculate the H_2 fraction of cold gas (Blitz & Rosolowsky 2006). To infer the H I and H_2 masses of a galaxy we only use the galaxy stellar mass, SFR, and size as input parameters. We pick a gas mass, distribute the gas as explained in the next paragraph, and then calculate a SFR for that gas mass following the equations given below. We repeat this process while iterating through gas masses till convergence with the observed SFRs is reached. When convergence is reached we separate the cold gas mass into an atomic and molecular component using equation 3.

We assume the galaxy stellar mass to be distributed following a Sérsic profile $\Sigma_*(r) \propto \exp[-(r/r_*)^{1/n}]$, where r_* is the scale radius of the stellar disc for a Sérsic profile and n the Sérsic index of the galaxy. We also assume that the gas in galaxies is distributed following the same Sérsic profile, with a scale radius

$$r_{\rm gas} = \chi_{\rm gas}\, r_*, \tag{1}$$

where $\chi_{\rm gas}$ is the scale radius of the gas disc relative to the stellar disc. We take $\chi_{\rm gas} = 1.7$ based on a fit to the galaxy disc profiles presented in Leroy et al. (2008).

We use a slightly adapted version of the star formation law deduced by Bigiel et al. (2008) to allow for higher star formation efficiencies in high gas surface density regions. This is based on the results of Daddi et al. (2010) and Genzel et al. (2010), who found the star-formation at high surface densities to follow the KS relation (a power-law slope of 1.4 versus 1.0 for Bigiel et al. 2008). The resulting equation is given by

$$\Sigma_{\rm SFR} = \frac{A_{\rm SF}}{10 M_\odot\,{\rm pc}^{-2}} \left(1 + \frac{\Sigma_{\rm H2}}{\Sigma_{\rm crit}}\right)^{N_{\rm SF}} f_{\rm H_2}\, \Sigma_{\rm gas} \tag{2}$$

where $\Sigma_{\rm SFR}$ and $\Sigma_{\rm gas}$ are the star formation and cold gas surface densities in $M_\odot\,{\rm yr}^{-1}\,{\rm kpc}^{-2}$ and $M_\odot\,{\rm pc}^{-2}$, respectively; $A_{\rm SF}$ is the normalization of the power law in $M_\odot\,{\rm yr}^{-1}\,{\rm kpc}^{-2}$; $\Sigma_{\rm crit}$ is a critical surface density; $N_{\rm SF}$ is an index which sets the efficiency; and $f_{\rm H_2} = \Sigma_{\rm H_2}/(\Sigma_{\rm HI} + \Sigma_{\rm H_2})$ is the molecular gas fraction. Following Popping et al. (2012) we use $N_{\rm SF} = 0.5$ and we take $\Sigma_{\rm crit} = 70\, M_\odot\,{\rm pc}^{-1}$.

We use a pressure-regulated recipe to determine the molecular fraction of the cold gas, based on the work by Blitz & Rosolowsky (2006). They found a power-law relation between the mid-plane pressure acting on a galaxy disc and the ratio between molecular and atomic hydrogen, i.e.,

$$R_{\rm H_2} = \left(\frac{\Sigma_{\rm H_2}}{\Sigma_{\rm HI}}\right) = \left(\frac{P_m}{P_0}\right)^{\alpha} \tag{3}$$

where P_0 is the external pressure in the interstellar medium where the molecular fraction is unity; α is the power-law index; and P_m is the mid-plane pressure acting on the galaxy disc. We adopted $P_0 = 3.25 \times 10^{-13}{\rm erg\,cm}^{-3}$ and $\alpha = 0.8$ from Leroy et al. (2008). The mid-plane pressure can be described by (Elmegreen 1989)

$$P_m(r) = \frac{\pi}{2}\, G\, \Sigma_{\rm gas}(r)\, [\Sigma_{\rm gas}(r) + f_\sigma(r)\Sigma_*(r)] \tag{4}$$

where G is the gravitational constant, r is the radius from the galaxy centre, and $f_\sigma(r)$ is the ratio between $\sigma_{\rm gas}(r)$ and $\sigma_*(r)$, the gas and stellar vertical velocity dispersion, respectively. Following Fu et al. (2010), we adopt $f_\sigma(r) = 0.1\sqrt{\Sigma_{*,0}/\Sigma_*}$, where $\Sigma_{*,0} \equiv m_*/(2\pi r_*^2)$, based on empirical scalings for nearby disc galaxies. Putting this together, we have an expression for the star formation surface density in Equation (2) depending on the cold gas surface density and stellar mass surface density. We integrate the SFRs in the individual annuli to obtain a total SFR which can be compared to the observed SFR.

We calibrated our method using direct observations of the H I and/or H_2 content of galaxies in the local and high-redshift Universe from Leroy et al. (2008), Daddi et al. (2010), Tacconi et al. (2010), and Tacconi et al. (2013)[1]. Using χ^2-minimization, we find the best agreement between predicted and observed gas masses when adopting a value of $A_{\rm SF} = 9.6 \times 10^{-3}\, M_\odot\,{\rm yr}^{-1}\,{\rm kpc}^{-2}$. This value is close to normalizations found in Bigiel et al. (2008) and Bigiel et al. (2011), 8.42×10^{-3} and $4.6 \times 10^{-3}\, M_\odot\,{\rm yr}^{-1}\,{\rm kpc}^{-2}$, respectively. We integrate the gas disc out to 10 times $r_{\rm gas}$. We discuss the uncertainties on some of the individual components of this model in Section 4. The typical systematic uncertainty of our method is 0.3 dex.

A schematic picture of the dependencies of our model is presented in Figure 1. In this figure we explore the effects of changing one of the three input properties of a galaxy (SFR, size, and stellar mass) on the estimated cold gas mass and H_2 mass of a galaxy and the cold gas fraction ($f_{\rm gas}$) and molecular hydrogen fraction of the cold gas ($f_{\rm H2}$). We keep two of the parameters fixed and vary the third. Changing the stellar mass of the galaxy has a negligible effect on the inferred cold gas and H_2 mass. It is only for the most massive galaxies ($M_* \approx 10^{11}\,{\rm M}_\odot$) that, due to the increased pressure from stars, the inferred cold gas mass decreases and $f_{\rm H2}$ increases. Because the inferred cold gas mass remains relatively constant, the cold gas fraction $f_{\rm gas}$ rapidly decreases with increasing stellar mass.

We find a strong increase in cold gas mass, H_2 mass, $f_{\rm gas}$, and $f_{\rm H2}$ when increasing the SFR. This is not surprising, as more gas is needed to support the higher SFR. The increased gas mass enhances the cold gas surface density and pressure acting on the gas, which leads to an increase in $f_{\rm H2}$.

The inferred gas masses increase as a function of scale radius. When increasing the scale radius, the gas densities decrease, therefore the molecular fraction of the gas decreases and the SFR surface density decreases as well. To ensure that convergence with the input SFR is obtained, more gas has to be added to the galaxy to make up for the lowered H_2 fractions. This results in high gas fractions and low molecular hydrogen fractions.

2.2 Data

We infer the galaxy gas content of two deep samples of F160W (H-band) selected galaxies from the CANDELS survey at $0.5 < z < 3$ (Grogin et al. 2011; Koekemoer et al.

[1] Leroy et al. (2008),Tacconi et al. (2010), and Tacconi et al. (2013) assume a CO-to-H_2 conversion factor of $X_{\rm CO} = 2 \times 10^{20}{\rm cm}^{-2}/({\rm K\,km\,s}^{-1})$. Daddi et al. (2010) assumes a CO-to-H_2 conversion factor of $X_{\rm CO} = 2.25 \times 10^{20}{\rm cm}^{-2}/({\rm K\,km\,s}^{-1})$

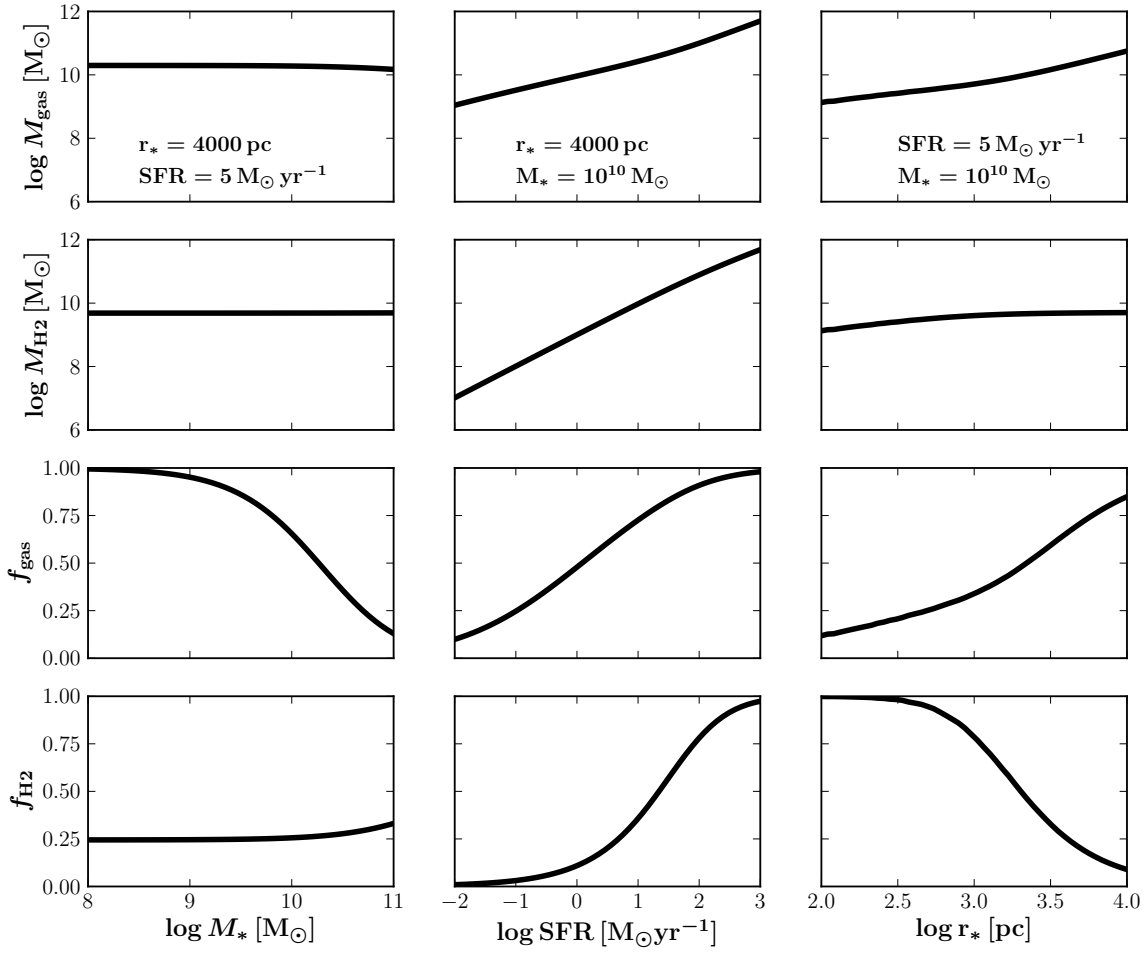

Figure 1. Schematic change in cold gas mass, H_2 mass, cold gas fraction ($f_{\rm gas} \equiv M_{\rm gas}/(M_{\rm gas}+M_*)$) and molecular hydrogen fractions ($f_{\rm H2} \equiv M_{\rm H2}/M_{\rm gas}$) produced by our model when varying the stellar mass (left column), SFR (middle column) and scale radius (right column) of a galaxy. For each column the other two of three input galaxy properties of our model (stellar mass, SFR, and scale radius) are fixed. The fixed values are quoted in the upper panels.

2011). One of the samples corresponds to the Great Observatories Origins Deep Survey South (GOODS-S; Giavalisco et al. 2004), and the other to the UKIDSS Ultra-Deep Survey (UDS) field (Lawrence et al. 2007). We used the publicly available CANDELS photometric catalogues compiled by Guo et al. (2013) and Galametz et al. (2013), and the redshift compilation by Dahlen et al. (2013), with spectroscopic redshift updates taken from Fadda et al. (2010) and Barro et al. (2014), to select our galaxies. We selected disc galaxies based on their Sérsic index and excluded galaxies that contain an active galactic nucleus (AGN). We did not apply any selection based on stellar mass or SFR. The exact selection criteria and our methods to calculate stellar masses, SFRs, and sizes are described below.

As our method requires us to know the scale radius of each galaxy, we extracted from these catalogues all those sources with good-quality morphological fits in the H band, as determined by van der Wel et al. (2012). We computed the circularized, effective radius r_e of a galaxy as $r_e = a_e\sqrt{(b/a)}$, where a_e is the effective radius along the major axis and b/a the ratio between the minor and major axis sizes and converted these to the scale length r_* for a Sérsic profile with Sérsic index n. We converted all scale radii to a common rest-frame wavelength of 5000 Å following van der Wel et al. (2014). Since our model is designed for disc galaxies, we discarded all galaxies with a Sérsic index $n > 2.5$.

We excluded galaxies known to contain an AGN from our sample, to avoid any bias in the derived star formation rates and stellar masses. To identify AGN, we used the 4Ms Chandra X-ray catalogue for the GOODS-S field (Xue et al. 2011), and an infrared power-law spectral energy distribution analysis (Caputi 2013) in the UDS field, as the existing X-ray data is shallow (Ueda et al. 2008). These AGN constitute only 1–2% of the CANDELS $0.5 < z < 3$ samples. It is possible that other galaxies containing an AGN remained in our sample, but the AGN is likely weak as it is not identified in the X-ray data or with the IRAC power-law criterion.

By applying these morphology and AGN cuts, we kept around 60% of the galaxies in the GOODS-S and UDS CANDELS catalogues. The distributions of the H-band magni-

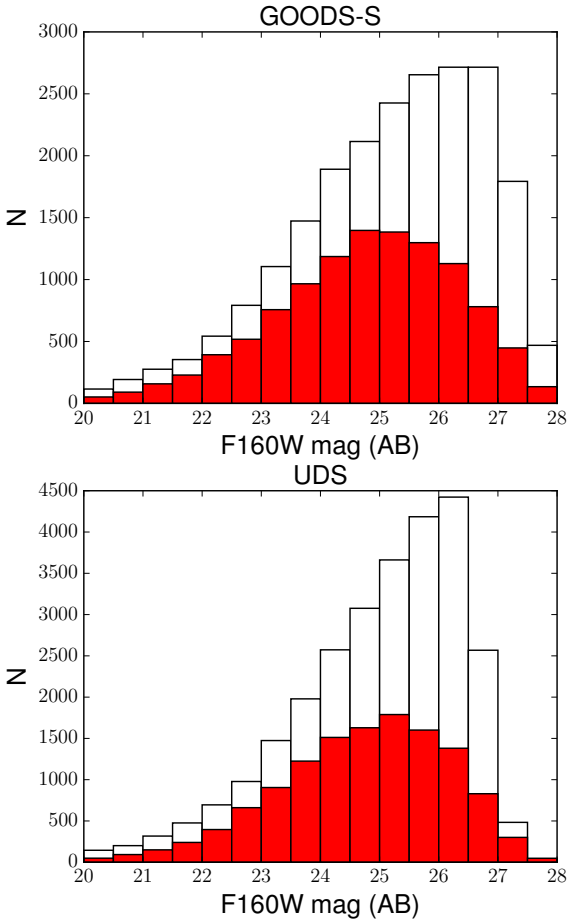

Figure 2. H-band magnitude distributions of the original (white) and final samples (after the morphology cut; red) at redshifts $0.5 < z < 3$ for the GOODS-S (top) and UDS (bottom) fields.

tudes of the original and final samples at $0.5 < z < 3$ for the two fields separately are compared in Fig. 2. From this Figure, we can see that 1) the GOODS-S sample reaches around a magnitude deeper than the UDS sample, as the former is based on both the deep and ultra-deep CANDELS data for the GOODS-S field; and 2) the percentage of galaxies lost because of the good-quality morphology cut and cut in Sérsic index is not constant with H-band magnitude. This cut still contains $> 50\%$ of the original galaxies for $H < 26$, but the sampling becomes progressively more sparse at fainter magnitudes. The depth of the GOODS-S sample reflects itself in a relatively higher number of low-stellar mass galaxies. Nevertheless, our sample is likely to miss extended galaxies with low surface brightness. This becomes especially important for galaxies with low stellar masses at $z > 2$. For our model this means that we are biased against low surface brightness galaxies (Guo et al. 2013).

We computed stellar masses using a multi-wavelength SED χ^2 fitting to the CANDELS photometry (from the U to the 4.5 μm band), applying the Bruzual (2007) templates fixed at the redshifts of the sample objects. We used a single stellar population and five exponentially-declining star formation histories (with τ = 0.1, 0.5, 1.0, 2.0, and 5.0 Gyr). For each star formation history we considered 24 possible templates, corresponding to ages between 0.05 and 5.0 Gyr. The Bruzual (2007) templates have a larger contribution from thermally pulsing asymptotic giant branch (TP-AGB) stars than the Bruzual & Charlot (2003) templates. Stellar masses calculated based on Bruzual (2007) are on average 0.1 dex less massive than stellar masses calculated based on the Bruzual & Charlot (2003) models. Internal dust extinction has been taken into account by convolving all Bruzual and Charlot templates with the Calzetti et al. (2000) reddening law, with A_v values ranging from 0.0 to 3.0 (with a step of 0.1).

SFRs are based on rest-frame UV fluxes corrected for extinction E(B-V) for each individual galaxy using the Calzetti et al. (2000) reddening law. UV fluxes were converted into SFRs following Kennicutt (1998a) for a Chabrier IMF. When IR photometry was available (for just a few percent of our sample) we calculated SFRs based on a combination of non-extinction corrected UV and IR photometry. We derived rest-frame 8μm luminosities from the 24μm fluxes, and converted the 8μm luminosities into total IR luminosities following Bavouzet et al. (2008). SFRs were calculated following Kennicutt (1998a) and Bell et al. (2005). In comparison with Popping et al. (2012) the CANDELS survey is closer to a mass-selected sample and (when IR photometry is available) is based on a more-reliable tracer of the SFR. As such, the results presented in this work supercede our previous efforts.

3 RESULTS

In this section we present galaxy SFRs and the inferred total cold gas, atomic hydrogen, and molecular hydrogen masses of galaxies in the CANDELS survey. We will focus on the gas masses, gas fractions, gas properties of galaxies and the evolution of the gas content of galaxies.

3.1 Galaxy SFR

To fully appreciate the predictive power of our model it is crucial to place the inferred gas masses in their proper context. Our cold gas and H_2 estimates depend on the SFR of a galaxy to first order. In Figure 3 we present the SFR of our galaxy sample as a function of stellar mass for different redshift bins. For clarity the relations are shown for the samples taken from the GOODS south field, the UDS field, and the combination of these fields. We find an increasing trend in SFR with stellar mass up to redshifts $z < 3$. The median of this trend has been referred to as the 'main sequence' of star-forming galaxies (e.g., Noeske et al. 2007; Elbaz et al. 2011). The normalization of the trend between stellar mass and SFR decreases with time. At fixed stellar mass, galaxies in the redshift range $2.5 < z < 3.0$ formed stars an order of magnitude more rapidly than in the redshift range $0.5 < z < 1.5$. At $0.5 < z < 1.0$ the increasing trend of SFR with stellar mass has a slope of 0.66. Other studies have found a slope ranging from 0.6 to 1 at the same redshifts (Pannella et al. 2009; Karim et al. 2011; Whitaker et al. 2012, 2014).

We did not apply any additional selection criteria beyond those described in Section 2.2. While many other studies only select galaxies on the 'main sequence' of star-

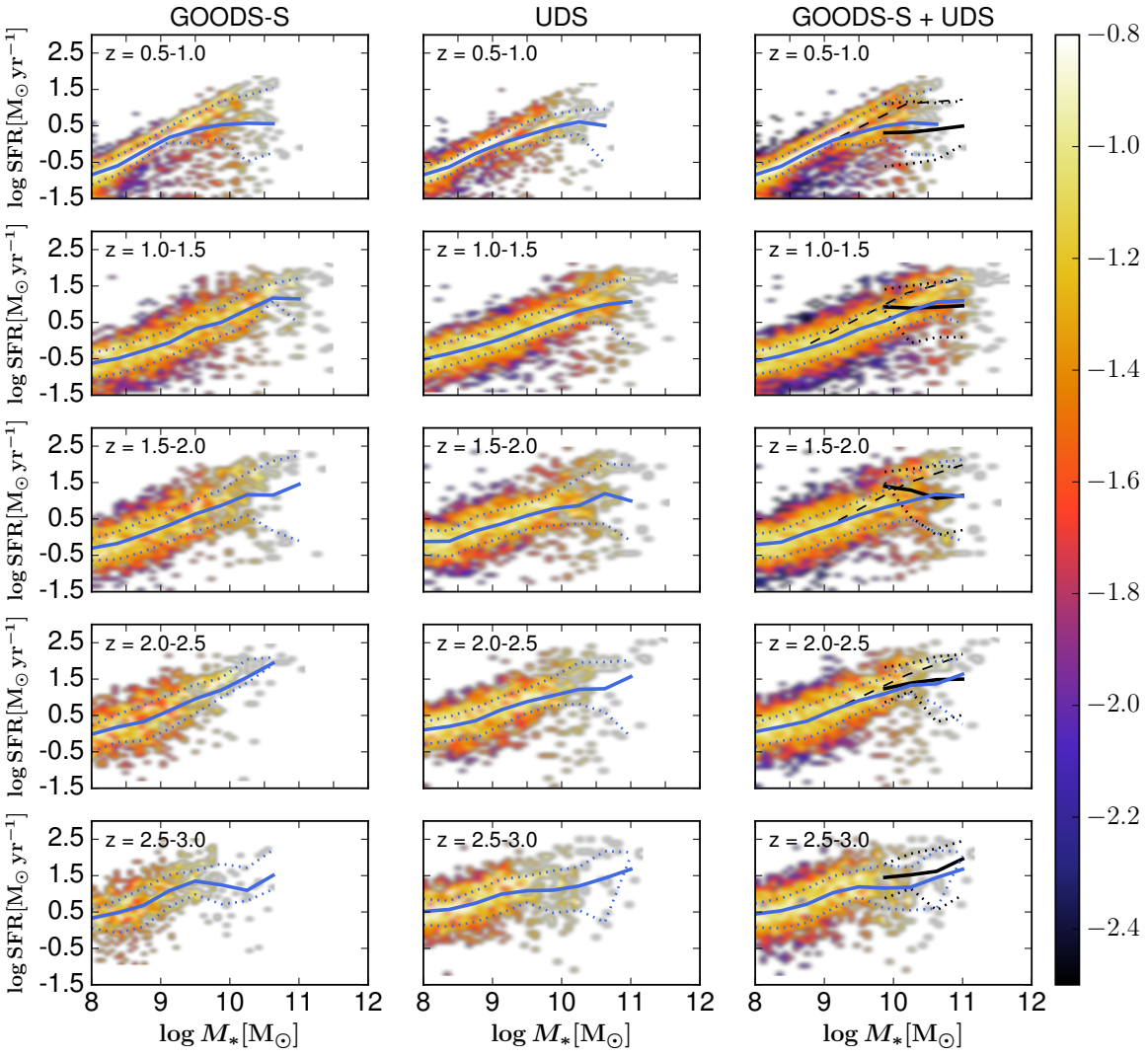

Figure 3. Galaxy SFR as a function of stellar mass in different redshift bins. The shaded regions show the log of the conditional probability distribution function $P(\mathrm{SFR}|M_*)$, which represents the probability distribution of SFRs for fixed stellar masses, and the blue solid and dotted lines show the median fit and 2σ deviation. The left column shows results for the GOODS-S sample, the middle column for the UDS sample, and the right column for the combined GOODS-S and UDS sample. The black line marks the mean trend of the UV + IR based SFRs presented in Barro et al. (2014) in the GOODS-S and UDS fields. The black dashed line mark the double-power-law fit to the relation between stellar mass and SFR presented in Whitaker et al. (2014).

formation, our sample also includes a fraction of galaxies with low SFRs.

We compare our SFRs with SFRs from Barro et al. (2014, black line in Figure 3) and the double power-law fit to the stellar mass – SFR relation presented in Whitaker et al. (2014, black dashed line). We find that our mean trends for the stellar mass – SFR relation are in reasonable agreement with trends found in the literature. We note that Barro et al. (2014) and Whitaker et al. (2014) applied criteria to select actively star-forming galaxies, attempting to exclude more quiescent objects, whereas our selection criteria do not rule out quiescent objects.

There is a large population of galaxies with stellar masses larger than $\sim 10^{10}\,M_\odot$ and low SFRs ($< 1.0\,\mathrm{M_\odot\,yr^{-1}}$). These galaxies with low SFRs are less actively forming stars than counterparts at fixed stellar mass and make up a group of quiescent galaxies (Brennan et al. 2015). For these stellar masses our sample is significantly incomplete (completeness < 50 per cent) below SFRs of $\log(\mathrm{SFR}/M_\odot\,\mathrm{yr}^{-1}) = -0.5$ at $z = 2$. The SFR limit to observe galaxies increases at higher redshifts. This implies that at redshifts $z > 2.0$ the contribution by galaxies with low SFRs may be larger.

3.2 Cold gas, H I, and H_2 content

We present the derived total cold gas masses of our galaxy sample as a function of stellar mass in different redshift bins

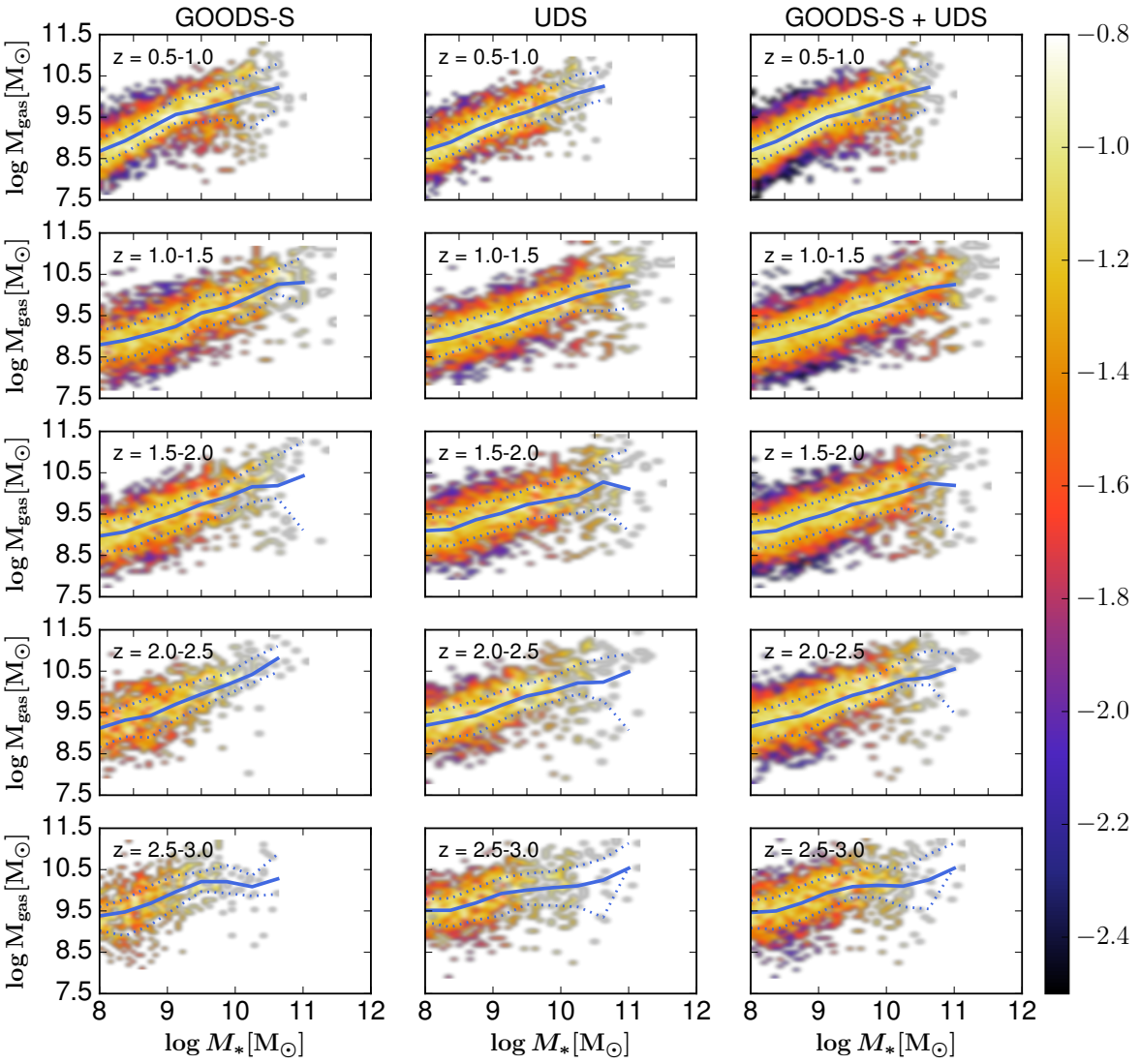

Figure 4. Total cold gas mass of galaxies as a function of their stellar mass in different redshift bins. The shaded regions show the log of the conditional probability distribution function $P(\mathrm{M_{gas}}|M_*)$, and the blue solid and dotted lines show the median fit and one σ deviation. Columns are as described in the caption of Figure 3.

in Figure 4. We find that on average the cold gas mass of a galaxy increases with its stellar mass at all observed redshifts with a sub-linear slope. Despite the clear increasing trend, we do find a significant amount of scatter. Note especially a group of gas-poor galaxies with high stellar masses. This group of galaxies seems to have decoupled itself from the general increasing trend of gas mass with stellar mass, indicating that some physical process has either removed some of the cold gas or prohibits the cooling and/or accreting of gas onto the galaxy. These galaxies are likely on their way towards the red sequence. There is a shift in the normalization in the relation between gas- and stellar-mass with redshift. On average, high-redshift galaxies (especially at $z > 2.0$) are more gas-rich than galaxies with similar stellar mass at lower redshifts. At $0.5 < z < 1.0$ the increasing trend of cold gas mass with stellar mass has a slope of 0.58.

We present the derived H_2 masses of our galaxy sample in five redshift bins in Figure 5. Similarly to the total cold gas mass, we find an increase in H_2 mass with stellar mass and a decrease in H_2 mass with decreasing redshift. We see a group of galaxies with high stellar masses and low H_2 masses at $z < 2.5$ in good agreement with a similar group of galaxies seen in the relation between cold gas and stellar mass (Fig. 4). The relation between H_2 mass and stellar mass is well defined and has a clear upper envelope over the entire range of stellar masses probed, with only minor stochastic appearance of galaxies above the envelope. The trend between H_2 mass and stellar mass is slightly steeper than for the total cold gas mass. At $0.5 < z < 1.0$ the increasing trend of H_2 mass with stellar mass has a slope of 0.65. Although the relations between stellar mass and cold

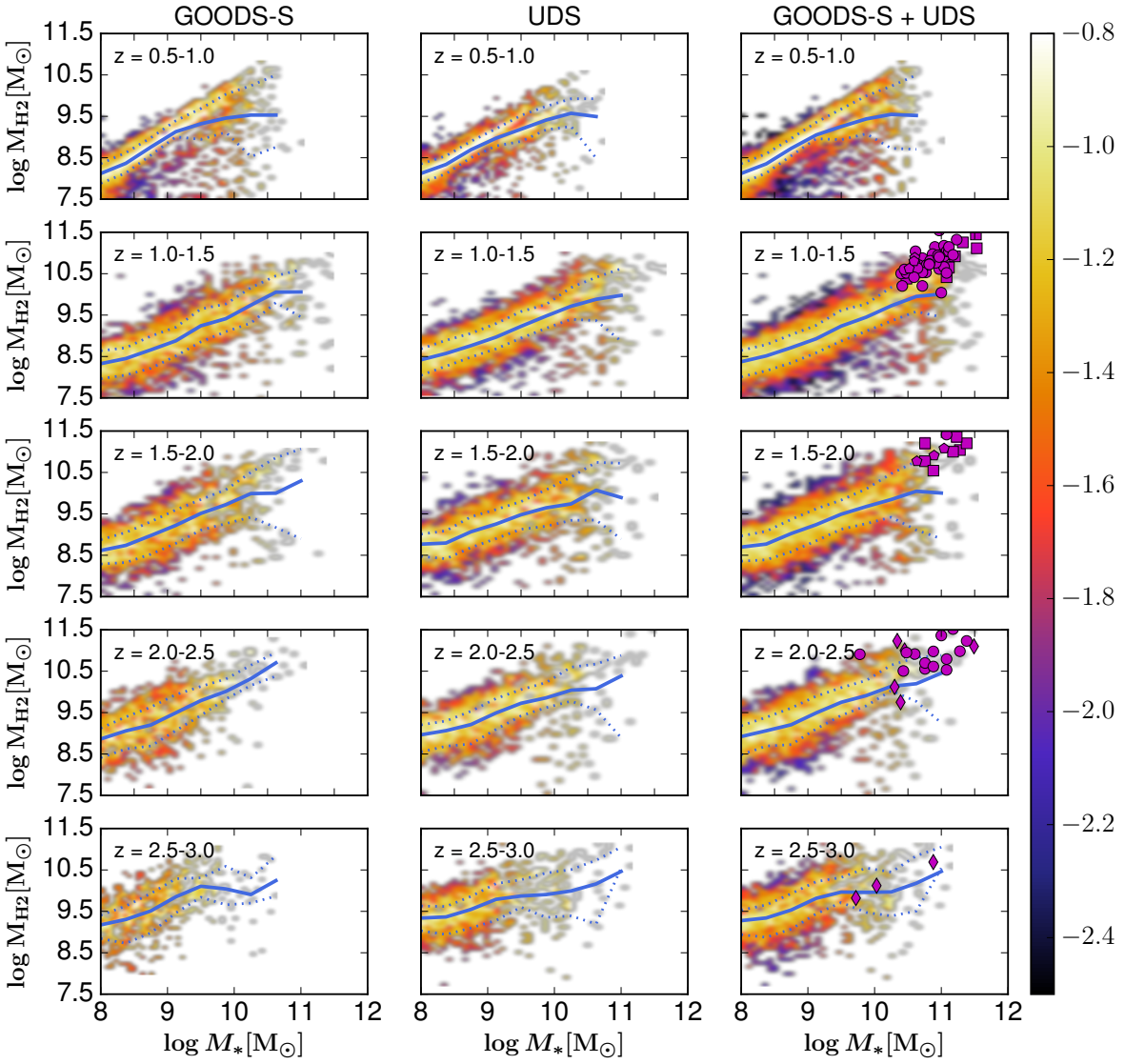

Figure 5. H_2 mass of galaxies as a function of their stellar mass different in redshift bins. The shaded regions show the log of the conditional probability distribution function $P(\mathrm{M_{H2}}|M_*)$, and the blue solid and dotted lines show the median fit and one σ deviation. Columns are as described in the caption of Figure 3. Purple pentagons, circles, squares, and diamonds are literature values from Daddi et al. (2010), Tacconi et al. (2010), Tacconi et al. (2013), and Saintonge et al. (2013), respectively.

and H_2 mass are very similar, there is no simple one-to-one mapping between cold gas mass and H_2 mass.

As a comparison we have included direct measures of the H_2 mass of galaxies (through their CO luminosity) from the literature (Tacconi et al. 2010; Saintonge et al. 2013; Tacconi et al. 2013) in Figure 5.[2] The mean trend for the inferred H_2 masses lies below the observed sample. Our sample contains 24000 galaxies covering four decades in stellar mass. The observational data points correspond to only a small number of galaxies in a very localized region of parameter space. Our sample was not selected to purely consist of 'main sequence' galaxies, driving the mean trends in inferred gas mass down with respect to a galaxy sample consisting of only 'main sequence' galaxies only. A close look at Figure 5 shows that most of the directly-observed H_2 masses are in good agreement with the most-H_2-massive (i.e., actively star-forming) galaxies at stellar masses $M_* > 10^{10}\,\mathrm{M_\odot}$. [3] We find that the increasing relation between stellar mass and H_2 mass suggested by the direct observations continuous at least down to stellar masses of $10^8\,\mathrm{M_\odot}$.

[2] Saintonge et al. (2013) calculates the CO-to-H_2 conversion factor as a function of metallicity using the prescription presented in Genzel et al. (2012).

[3] Tacconi et al. (2013) selected galaxies with a stellar masses $\geqslant 2.5\times10^{10}\,\mathrm{M_\odot}$ and star-formation rate$\geqslant 30\,\mathrm{M_\odot yr^{-1}}$. This matches the most-actively star-forming galaxies in our sample.

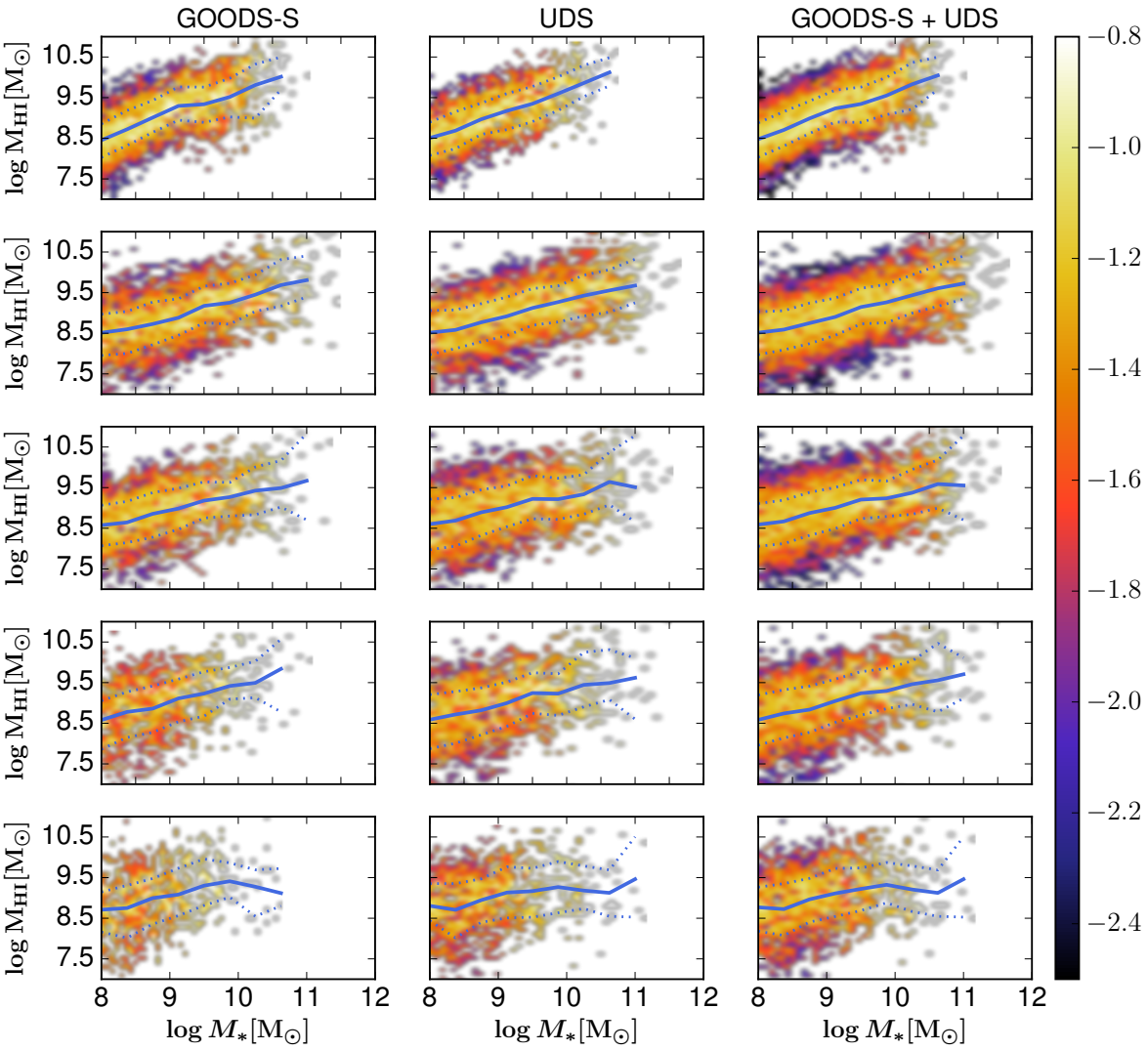

Figure 6. The H I mass of galaxies as a function of their stellar mass in different redshift bins. The shaded regions show the log of the conditional probability distribution function $P(\mathrm{M_{HI}}|M_*)$, and the blue solid and dotted lines show the median fit and one σ deviation. Columns are as described in the caption of Figure 3.

We show the H I mass of galaxies as a function of their stellar mass in different redshift bins in Figure 6. Like for the cold gas and H_2 mass, the H I content of galaxies increases as a function of stellar mass. The scatter around the mean trend is very wide, much wider than trends with cold gas mass and H_2 mass. At $0.5 < z < 1.0$ the trend between H I mass and stellar mass has a slope of 0.54.

The relations between stellar mass and cold gas, H I, and H_2 mass tightly follow the trend between SF and stellar mass (Figure 3). The well defined upper envelope of this relation for non-starburst galaxies is in good agreement with the upper envelope of the relation between stellar mass and H_2 mass. It is important to realize that in our model the H_2 mass is *to first order* a different representation of the SFR of a galaxy (through $A_{\rm SF}$), hence the similarity between the slopes of the relation of SFR and H_2 mass with stellar mass (0.66 for SFR versus 0.65 for the H_2 mass at $z = 0.5 - 1.0$). The total cold gas mass and H I mass are driven through a more complex combination of stellar mass, SFR and disc size, and therefore do not necessarily have a simple relationship with SFR. This is reflected in the difference in the slopes of the relations between stellar mass and SFR (slope of 0.66), cold gas mass (slope of 0.58), and H I (slope of 0.54). The inferred cold gas mass has a slightly shallower increase with stellar mass than the inferred H_2 mass and SFR.

3.3 Gas fractions

In Figure 7 we show galaxy gas fractions as a function of stellar mass and redshift. There is a strong anti-correlation between galaxy stellar mass and gas fraction at $z < 2.5$. The cold gas fraction remains relatively constant at stellar masses $M* \leqslant 10^{9.5}\,\mathrm{M}_\odot$ and drops rapidly at higher stellar

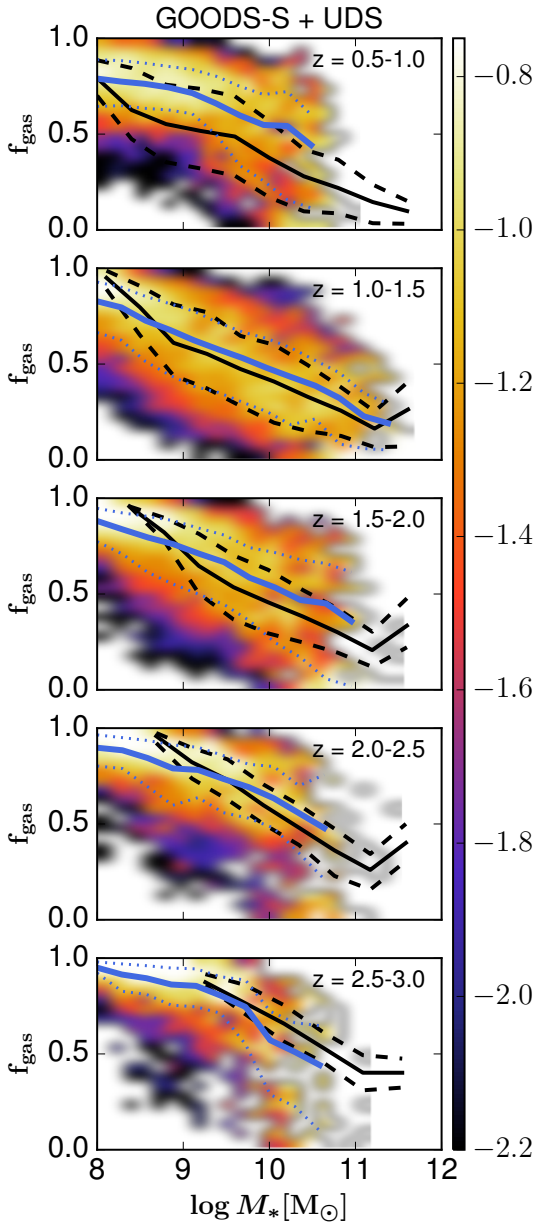

Figure 7. Cold gas fraction of galaxies ($f_{\rm gas} \equiv \frac{M_{\rm H2+HI}}{M_{\rm H2+HI}+M_*}$) as a function of stellar mass and redshift. The shaded regions show the log of the conditional probability distribution function $P(f_{\rm gas}|M_*)$, and the blue solid and dotted lines show the median fit and one σ deviation. The black solid and dashed lines show the mean fit and one σ deviation to the predictions of Popping, Somerville & Trager (2014).

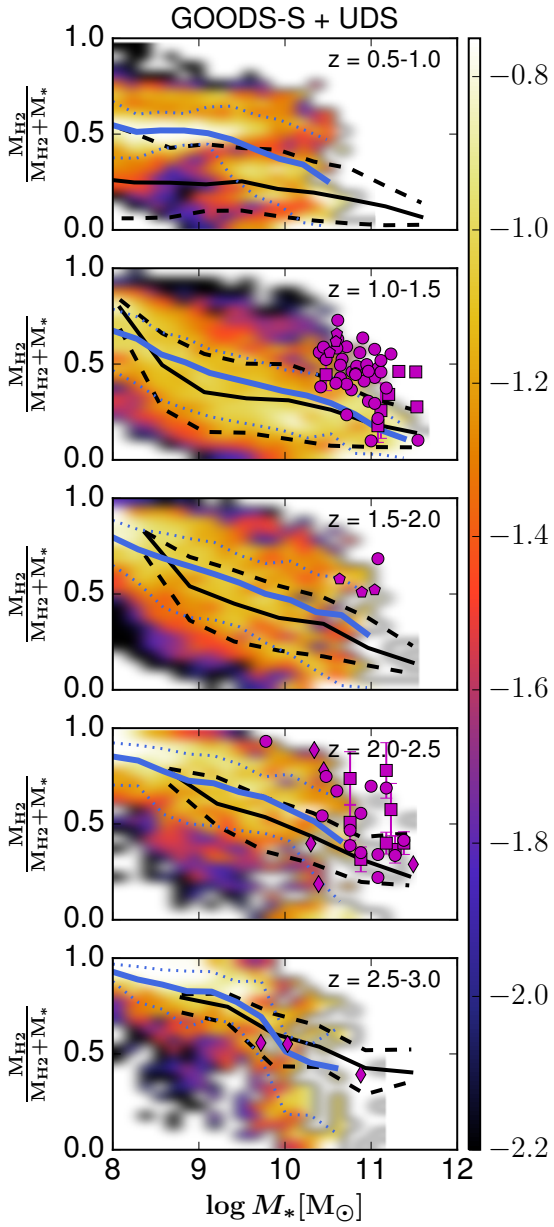

Figure 8. Relative molecular content as a function of stellar mass for different redshift bins. The shaded region shows the log of the conditional probability distribution function $P(\frac{\rm M_{H2}}{\rm M_{H2}+M_*}|M_*)$, and the blue solid and dotted lines show the median fit and one σ deviation. The black solid and dashed lines show the mean fit and 1 σ deviation to the predictions of Popping, Somerville & Trager (2014). Purple pentagons, circles, squares and diamonds are literature values from Daddi et al. (2010), Tacconi et al. (2010), Tacconi et al. (2013), and Saintonge et al. (2013), respectively.

masses for galaxies in our highest redshift bin ($2.5 < z < 3.0$). In the lower redshift bins the trend between stellar mass and cold gas fractions is roughly linear, mainly driven by a decrease in the cold gas fractions of galaxies with stellar masses $10^{9-10}\,M_\odot$. The characteristic mass above which the gas fractions rapidly drop ($M_* \approx 10^{9.5-10}\,{\rm M}_\odot$) suggests that some physical process prevents the buildup of large gas reservoirs in galaxies with a stellar mass above this characteristic mass, and is similar to the quenching mass scale (Kauffmann et al. 2003). We find the strongest evolution in galaxy cold-gas fraction in intermediate mass galaxies ($10^{9-10}\,M_\odot$). At a fixed stellar mass, a galaxys cold-gas fraction decreases with time.

We present $f_{\rm H2*} = \frac{M_{\rm H2}}{M_{\rm H2}+M_*}$ as a function of galaxy mass in Figure 8. This quantity is often used as an observable tracer of the gas content of galaxies. Similar to the total cold-gas fraction, there is an anti-correlation between H_2 and galaxy stellar mass, as well as redshift. High stellar mass

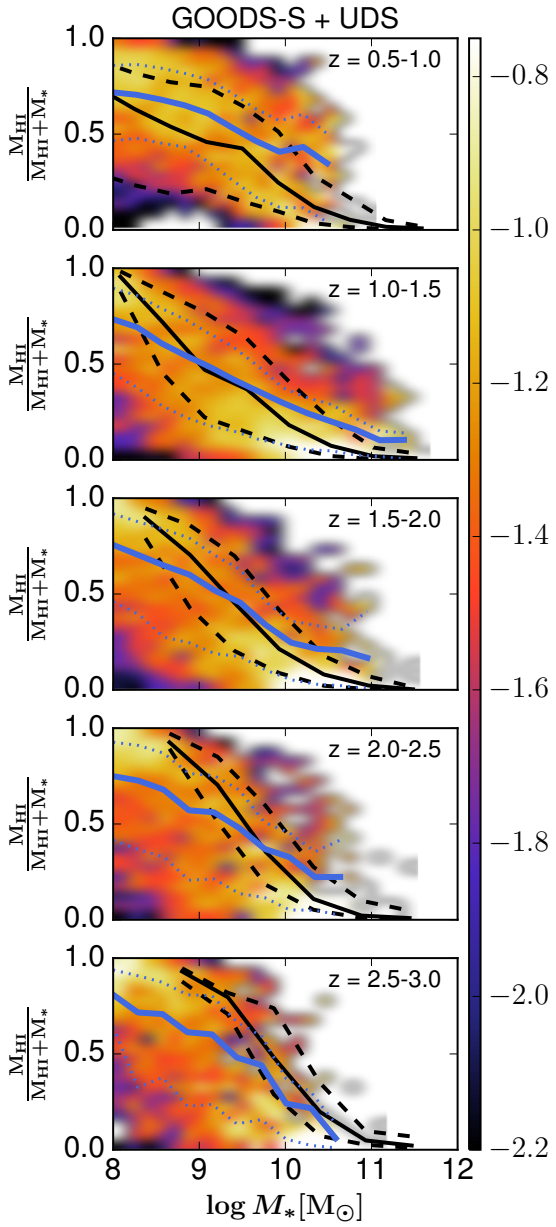

Figure 9. Relative atomic hydrogen content as a function of stellar mass for different redshift bins. The shaded region shows the log of the conditional probability distribution function $P(\frac{M_{HI}}{M_{HI}+M_*}|M_*)$, and the blue solid and dotted lines show the median fit and one σ deviation. The black solid and dashed lines show the mean fit and 1 σ deviation to the predictions of Popping, Somerville & Trager (2014).

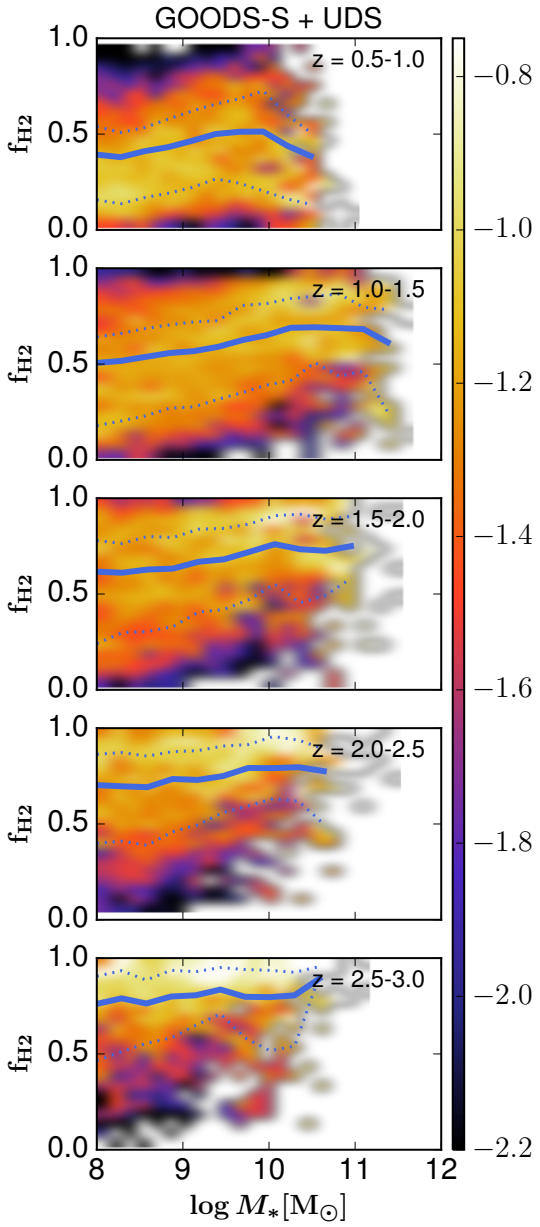

Figure 10. Molecular fraction ($f_{H2} \equiv M_{H2}/M_{gas}$) of the cold gas as a function of stellar mass for different redshift bins. The shaded region shows the log of the conditional probability distribution function $P(\frac{M_{H2}}{M_{gas}+M_*}|M_*)$, and the blue solid and dotted lines show the median fit and one σ deviation.

galaxies have on average the lowest relative H_2 content, and f_{H2*} decreases with redshift at a fixed stellar mass. The trend in f_{H2*} with stellar mass is similar to that for total cold-gas fraction.

We compare the results of our model with direct observations (through CO) of f_{H2*} in star-forming galaxies from Tacconi et al. (2010), Saintonge et al. (2013), and Tacconi et al. (2013). Although direct observations of f_{H2*} do not lie on top on the mean trend, they are in good agreement with the most massive and H_2-rich galaxies in our sample. As discussed when we described Figure 5, the difference between the mean trend and observations is driven by different selection criteria. Tacconi et al. (2013) developed a formalism to correct gas fractions for this selection effect and found gas fractions of ∼30 per cent at $z = 1 - 1.5$ for galaxies with stellar masses $\sim 10^{11} M_\odot$, in reasonable agreement with our inferred gas fractions.

We present the relative amount of atomic hydrogen in galaxies ($f_{HI*} = \frac{M_{HI}}{M_{HI}+M_*}$) as a function of stellar mass for different redshift bins in Figure 9. Similar to the previous figures, f_{HI*} decreases with stellar mass. Below stellar masses of $\sim 10^9 M_\odot$ the H I mass of galaxies exceeds the stellar

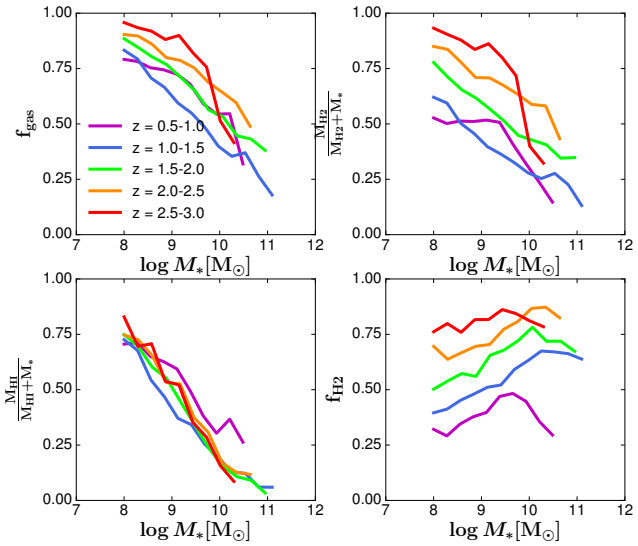

Figure 11. Evolution of the mean trends in $f_{\rm gas}$, $f_{\rm H2*}$, $f_{\rm HI*}$, and $f_{\rm H2}$ as a function of stellar mass. Note that the mean trend in $f_{\rm HI*}$ with stellar mass remains constant with time, whereas the other three properties do evolve.

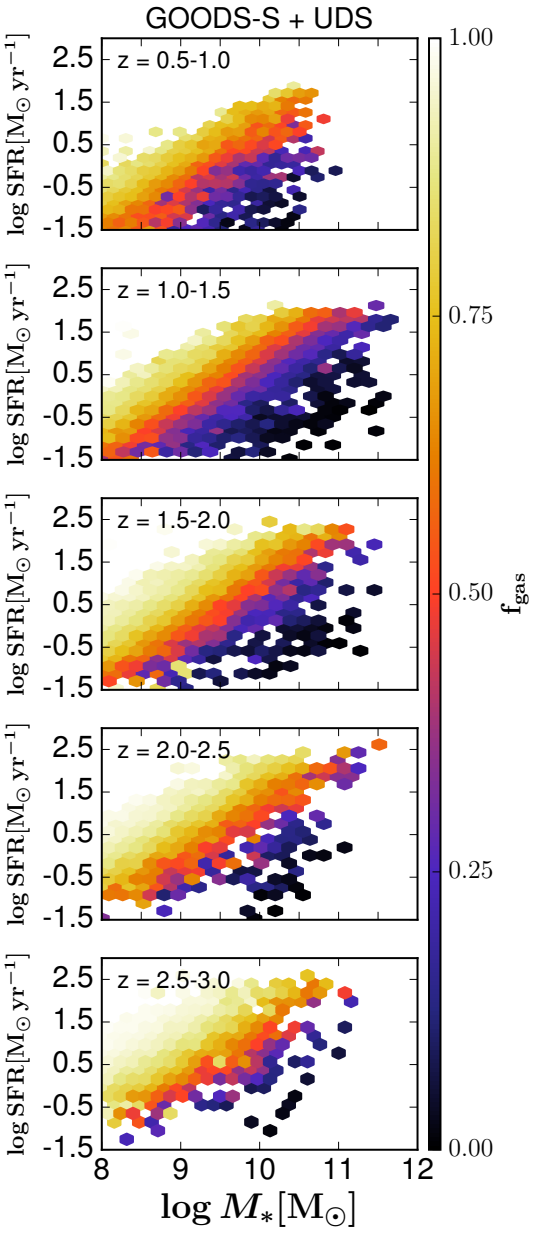

Figure 12. Galaxy SFR as a function of stellar mass for different redshift bins. The colour map gives the cold gas fraction of the galaxies. Each galaxy is counted only once to create the hexagons.

mass, whereas at higher stellar mass the H I mass is less than the stellar mass. Interestingly, there does not seem to be a strong evolution in the trend between $f_{\rm HI*}$ and stellar mass with time. A similar transition mass from H I to stellar mass dominated is seen for local galaxies (e.g., Cortese et al. 2011; Huang et al. 2012).

In Figure 10 we present the molecular fraction of the cold gas ($f_{\rm H2} \equiv M_{\rm H2}/M_{\rm gas}$) as a function of stellar mass for different redshift bins. This is a good measure of the fraction of gas available for SF as a function of time. The relation between $f_{\rm H2}$ and stellar mass is relatively flat at $z > 2.5$. We find an increasing trend between $f_{\rm H2}$ increasing with stellar mass towards lower redshifts. We find that $f_{\rm H2}$ increases with stellar mass up to a stellar mass of $\sim 10^{10}$ M$_\odot$ and decreases at higher stellar masses in our lowest redshift bins ($0.5 < z < 1.0$). The average H_2 fraction of galaxies decreases with time at fixed stellar mass (only at $M_* > 10^{10}$ M$_\odot$ do galaxies at $2.0 < z < 2.5$ have higher $f_{\rm H2}$ than at $z > 2.5$). This result clearly shows that both the cold gas and H_2 reservoirs decrease with time, although not necessarily at the same rate. It is important to note that the relation between stellar mass and H_2 fraction has a large scatter, especially at low stellar masses and lower redshifts. There is no well defined drop in H_2 fraction at a characteristic stellar mass and/or time.

We show the mean trends of the previous four Figures again in Figure 11, with the aim of focusing on the evolution of these trends. We find the remarkable result that $f_{\rm gas}$, $f_{\rm H2*}$, and $f_{\rm H2}$ all decrease as a function of time, whereas $f_{\rm HI*}$ remains nearly constant. Although the gas content of galaxies at fixed stellar mass decreases as a function of time, the changed partitioning of cold gas in H I and H_2 results in a constant fraction of H I in galaxies with fixed stellar mass. We discuss this further in Section 5.

The CANDELS results suggest a gradual evolution in the cold gas fraction and the relative molecular hydrogen content of galaxies at $0.5 < z < 3$, independent of stellar mass.

3.3.1 *Model comparison*

As a comparison we included predictions from the semi-analytic model presented in Popping, Somerville & Trager (2014) in Figures 7, 8, and 9. We ran the models in the appropriate redshift bins and applied a CANDELS selection criteria to the model output ($H_{\rm AB} < 26$). We only selected disc-dominated galaxies (bulge-to-total ratio less than 0.4).

Although the results presented in this paper are merely model predictions, they are based on actual observables

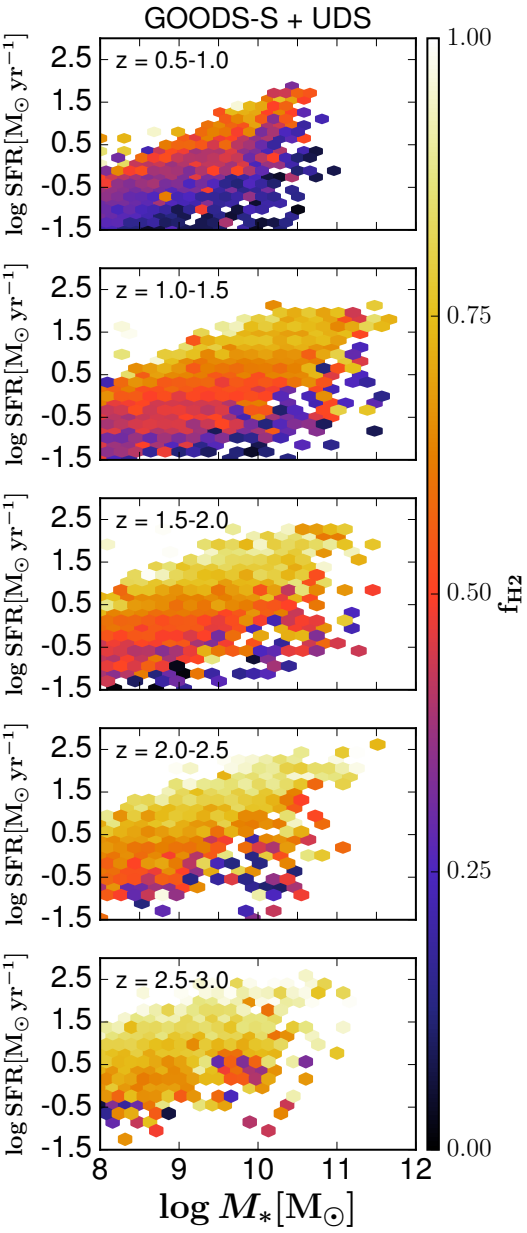

Figure 13. Galaxy SFR as a function of stellar mass for different redshift bins. The colour map gives the molecular fraction of the cold gas.

rather than introducing uncertain recipes describing the physics acting on galaxies. A comparison between the results presented in this work and semi-analytic predictions can shed light on the successes and failures of theoretical models. We acknowledge that the results presented are effectively a different representation of the phase space described by stellar mass, SFR, and galaxy size. One could therefore also compare the observed values for these quantities to semi-analytic model predictions. Nevertheless, focusing on the gas masses of galaxies and potential discrepancies between the results presented in this work and semi-analytic model predictions may provide a more direct hint of the baryonic physics that need to be changed and/or included for models to reach better agreement with observations. Somerville & Davé (2014) showed that semi-analytic models and hydrodynamic models predict too little SF in galaxies at redshifts $z = 1$ and $z = 2$ (for a potential solution see Henriques et al. 2014; White, Somerville & Ferguson 2015). Our method has the potential to assess whether this is due to too low gas masses in general or too little H_2.

The semi-analytic model predictions are in good qualitative agreement with our inferred cold gas fractions at redshifts $z = 0.5$ to $z = 2.5$ (Figure 7). We predict up to 10 per cent more cold gas in galaxies with stellar masses larger than $10^{10}\,M_\odot$ than the semi-analytic model. At higher redshift the semi-analytic model predicts gas fractions higher than found in this work for galaxies with stellar masses larger than $10^{10}\,M_\odot$.

Semi-analytic model predictions are in good qualitative agreement with our inferred H_2 masses at redshifts $1 < z < 1.5$ (Figure 8). At lower redshifts the semi-analytic model predicts much less molecular hydrogen than the results presented in this paper, whereas the model predict on average 1.8 times less molecular hydrogen at higher redshifts (f_{H2*} is approximately 10 per cent less). In the highest-redshift bin the model overpredicts f_{H2*} compared to the inferred fractions at $M_* > 10^{10}\,M_\odot$, whereas it underpredicts the relative amount of H_2 in galaxies at lower stellar masses.

The Popping et al. semi-analytic model on average predicts higher values for f_{HI*} at stellar masses less than $10^{10}\,M_\odot$ than the results presented in this work. The model also finds that at redshifts $z = 3 - 1$ the amount of H I in galaxies at fixed stellar mass remains relatively constant. We will further discuss the implications of this comparison in the discussion.

3.4 Gas properties on the stellar mass – SFR diagram

In Figure 12 we show the cold gas fraction of galaxies on the stellar mass–SFR relation. We find that to first order, galaxy cold gas fractions are well parameterized by their stellar mass and SFR. It is important to realize that both the SFR and the stellar mass of a galaxy are key ingredients in our model that set a galaxy's cold gas mass and its partitioning into atomic and molecular hydrogen. Galaxy gas fractions stay constant parallel to the relation between SFR and stellar mass, increasing towards higher SFR and decreasing with stellar mass. The upper envelope in the stellar mass–SFR diagram is populated by the most gas-rich objects at a given stellar mass. Although counterintuitive, galaxies with the highest SFRs do not necessarily have the highest gas fractions. The highest gas fractions are found in galaxies with low stellar masses and high SFRs. Galaxies with high stellar mass and low SFRs have the lowest gas fractions. At a fixed position in the stellar mass–SFR diagram galaxy cold gas fractions decrease with time.

We explore the H_2 fraction of galaxies in the stellar mass–SFR plane in Figure 13. Molecular gas fractions increase with increasing SFR. The most actively star-forming galaxies have highest molecular gas fractions, and the least-actively star-forming galaxies have the lowest fractions. Molecular fractions cannot be parameterized by a simple

combination of stellar mass and SFR as the total cold-gas fractions.

More information can be obtained by comparing Figures 12 and 13. These figures clearly show that large *cold*-gas reservoirs do not necessarily lead to large *molecular*-gas reservoirs and active SF. This is especially evident for galaxies with low stellar mass ($\sim 10^8\,\mathrm{M}_\odot$) and SFR $\sim 1\,\mathrm{M}_\odot\,\mathrm{yr}^{-1}$ at $z < 1.5$. These galaxies are dominated by atomic gas. Despite being rich in cold gas, only approximately 25 per cent of their cold gas is molecular and available to form stars. These objects were below the observation limit of the galaxies in Popping et al. (2012). The deep near-IR photometry of the CANDELS survey allows us to study these atomic-gas-dominated low-mass galaxies. Observations of local galaxies show a similar decrease in H_2 fraction with decreasing stellar mass (Saintonge et al. 2011; Boselli et al. 2014; Bothwell et al. 2014), with on average even lower H_2 fractions than the galaxies in our sample.

The most actively star forming galaxies ($\sim 10^{11}\,\mathrm{M}_\odot$ and SFR $\sim 100\,\mathrm{M}_\odot\,\mathrm{yr}^{-1}$) at $z < 2.5$ have relatively small cold gas reservoirs ($\mathrm{f_{gas}} < 0.5$), but most of this cold gas is molecular. Galaxies with high stellar mass and low SFRs are nearly empty of cold gas, but the molecular fraction of this gas is approximately 0.5 and can account for some residual star-formation.

3.5 Gas properties on the stellar mass – size relation

We present the cold-gas and molecular fraction of galaxies on the stellar mass–size relation in Figures 14 and 15. Within our model the scale radius of a galaxy sets the surface densities that control the molecular fraction and the total mass of cold gas in that galaxy. At fixed stellar mass the cold gas fractions of star-forming galaxies increase with increasing size. The molecular fraction of the cold gas, on the other hand, decreases with increasing size. For a fixed scale radius the cold-gas fraction and molecular fraction of a galaxy decrease with time.

The largest variations in molecular fractions are found in low-stellar-mass galaxies ($M_* < 10^{10}\,M_\odot$). At higher stellar masses we find differences in molecular fraction of approximately 25 per cent. Although less dramatic than for lower-mass galaxies, such variations are still significant.

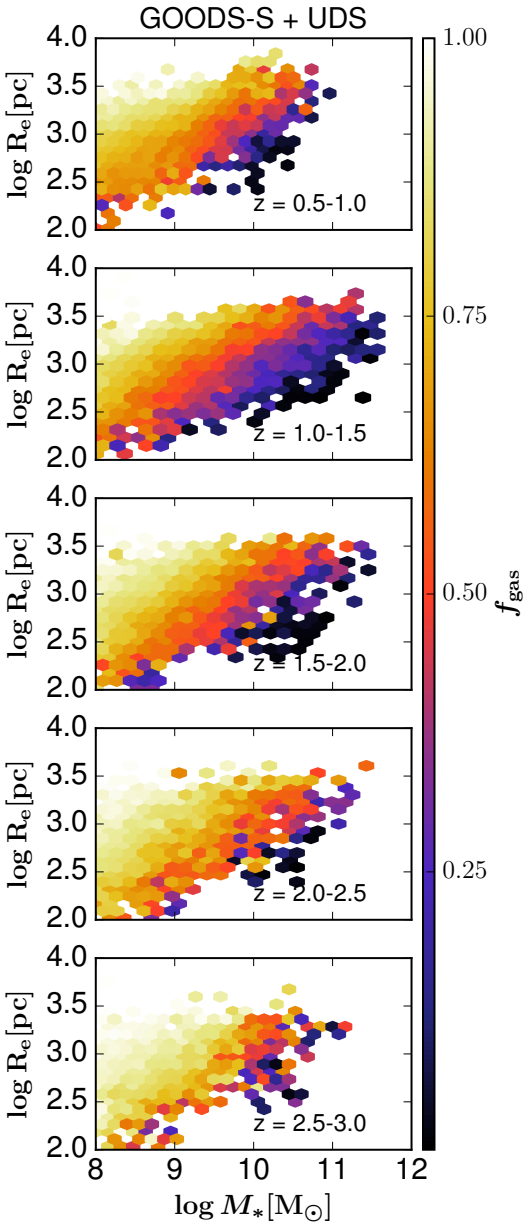

Figure 14. Galaxy scale radius as a function of stellar mass for different redshift bins. The colour map gives the cold gas fraction.

3.6 Star-formation efficiencies

The star-formation efficiency (the ratio between SFR and total cold gas mass (H I + H_2), i.e., SFE $\equiv$ SFR/$\mathrm{M_{gas}}$) is a good measure of how efficiently galaxies turn cold gas into stars.[4] We show the SFE of galaxies on the stellar mass–SFR and stellar mass–size diagrams in Figures 16 and 17.

We find that galaxy SFEs increase with increasing SFR and decrease with time. The SFE of galaxies that populate the upper envelope in the stellar mass–SFR relation changes as a function of stellar mass. At high stellar masses, galaxies are more than twice as efficient in forming stars out of their total cold gas reservoirs (H I + H_2) than at low stellar masses. This shows that the position of a galaxy on the stellar mass–SFR plane is being driven by the amount of cold gas available *and* by the ability of the gas to form molecules and stars (Saintonge et al. 2012; Genzel et al. 2014; Sargent et al. 2014). The group of galaxies with low SFRs at high stellar masses is more than twice as inefficient in forming stars than their counterparts with the same stellar mass that are actively forming stars. Overall, the SFE of galaxies decreases with time.

The SFE of galaxies decreases with increasing scale ra-

[4] We note that the star-formation efficiency of galaxies is often defined as the ratio between SFR and molecular hydrogen mass H_2 (i.e., SFE $\equiv$ SFR/$\mathrm{M_{H2}}$). Our adopted definition of the ratio between SFR and total cold gas mass is slightly different and important for simulations that do not discriminate between H I and H_2.

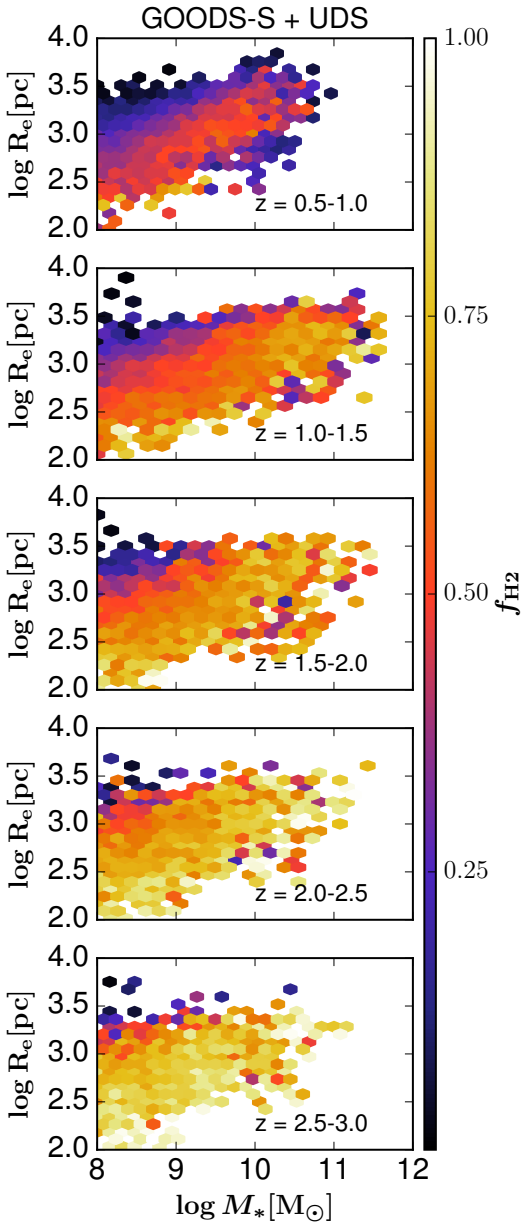

Figure 15. Galaxy scale radius as a function of stellar mass for different redshift bins. The colour map gives the molecular fraction of the cold gas. At fixed stellar mass more compact galaxies have higher molecular fractions.

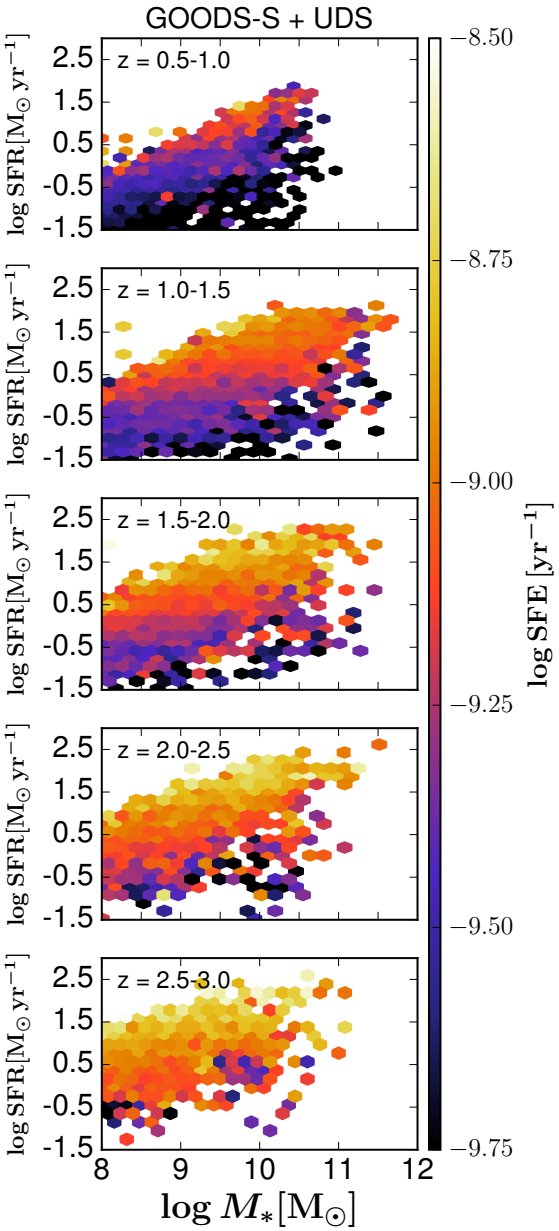

Figure 16. Galaxy SFR as a function of stellar mass for different redshift bins. The colour map gives the star-formation efficiency (SFE ≡ SFR/M_{gas}) of the galaxies.

dius. This is especially clear for galaxies with low stellar mass, but is also apparent for the most massive galaxies in our sample. This result is in good agreement with our findings in Figure 15. Compact galaxies have higher molecular fractions and are therefore more efficient at forming stars.

3.7 Global evolution of cold gas content of galaxies

The evolution of f_{H2*} with redshift has been studied in several different CO surveys and through dust continuum estimates (Geach et al. 2011; Tacconi et al. 2010; Daddi et al. 2010; Magdis et al. 2012; Tacconi et al. 2013; Saintonge et al. 2013; Bauermeister et al. 2013; Genzel et al. 2014; Scoville et al. 2014). These surveys suggest f_{H2*} increases with increasing redshift up to $z \sim 2$ and flattens or even declines at higher redshifts (Saintonge et al. 2013).

We present the evolution in f_{H2*} for galaxies with different selection criteria in stellar mass and SFR in Fig. 18 (top row). Our method allows us to infer the gas content for a large number of galaxies covering a wide range in physical properties (stellar masses, SFRs). This makes it ideal to investigate the effects that different selection criteria have on cold gas evolution trends inferred from direct observations of the CO emission line and the dust continuum of galaxies.

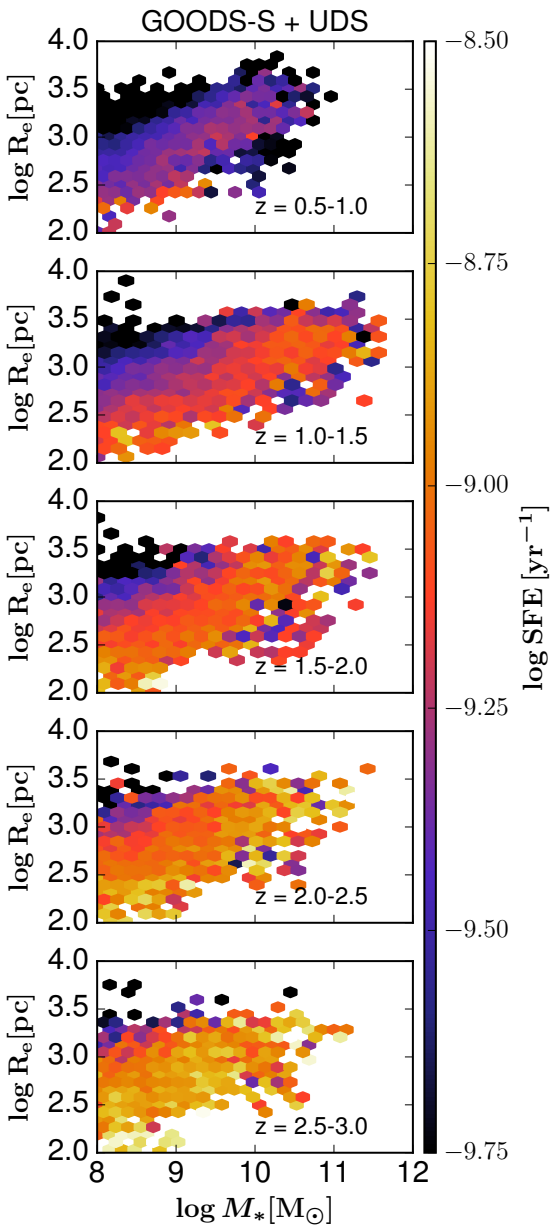

Figure 17. Galaxy scale radius as a function of stellar mass for different redshift bins. The colour map gives the star-formation efficiency (SFE $\equiv$ SFR/$M_{\rm gas}$) of the galaxies.

We find a decrease in the relative H_2 content of galaxies from $z \sim 3$ to $z \sim 1$. There is a minor increase in the relative H_2 content (and other fractions) from $z = 1.0$ to $z = 0.5$ when selecting galaxies with stellar masses larger than $10^9\,M_\odot$. Above $z = 2.0$ the evolution of $f_{\rm H2*}$ becomes less steep. This observed evolution is similar to the results presented in Saintonge et al. (2013). The normalization and the shape of the evolution in $f_{\rm H2*}$ depend on the selection criteria applied. We find the best match with the current direct observations when selecting only galaxies with SFR $> 30\,M_\odot\,{\rm yr}^{-1}$ for galaxies with stellar masses $\log(M_*/M_\odot) > 10.0$, similar to the selection limits of the observed samples. When loosening the selection criteria for SFR the normalization of $f_{\rm H2*}$ decreases. These galaxies with low SFRs are currently typically not accounted for in direct surveys of the molecular content of galaxies through either CO or FIR sub-mm continuum studies. When including galaxies with lower stellar masses we find that not only the normalization in the evolution of $f_{\rm H2*}$ increases, the slope of the decline in $f_{\rm H2*}$ at $z \leqslant 2$ also becomes stronger. We find no changes in the evolution of $f_{\rm H2*}$ when selecting galaxies with stellar masses more massive than 10^9 solar masses and changing the SFR criteria.

The relative amount of atomic hydrogen in galaxies slightly decreases with time in galaxies with stellar masses larger than $10^9\,M_\odot$ and remains constant in galaxies with stellar masses more massive than $10^{10}\,M_\odot$.

The mean molecular fraction f_{H2} of the cold gas in galaxies gradually decreases over the entire redshift range probed. This is in good agreement with the results presented in Figure 10 where we showed that the mean molecular fractions as a function of stellar mass decreases by approximately 25 per cent for the lowest mass galaxies from redshift 3 to 0.

4 MODEL ASSUMPTIONS AND APPLICABILITY TO THE CANDELS SAMPLE

The presented approach is based on several assumptions that may not always hold. In this section we discuss the main assumptions and how they affect our inferred gas masses.

We converted all the sizes to a common restframe wavelength of 5000 Å. Originally they were based on H band photometry. Across the $z = 0.5$–3 redshift range the H-band photometry spans a restframe size from the B band to the I band. Inferred gas masses based on the 5000 Å restframe morphology are slightly higher than based on the original H-band morphology. When adopting the 5000 Å restframe morphology, less than 5% of the galaxy sample is more than 10% more gas rich than when adopting the H-band morphology. Only a handful of objects is more than 20% more gas rich when adopting a 5000 Å morphology, rather than the H-band morphology.

A key assumption in our method is an exponential distribution of stars and gas in the galaxy discs. SF takes place in molecular clouds (local clumps in the disc not following an exponential distribution) which could lead to a local underestimation of the cold gas surface density. In this work we are averaging over ∼kpc scales and at our redshifts of interest and at these scales the exponential disc model is a good approximation to the stellar distribution of star-forming galaxies on galactic scales (Wuyts et al. 2011). Furthermore, analyses of local galaxies have revealed an exponential distribution of the cold gas in star-forming galaxies (Leroy et al. 2008; Bigiel & Blitz 2012; Kravtsov 2013; Wang et al. 2014).

Our model assumes a constant ratio between the gas and stellar disc scale lengths ($\chi_{\rm gas} = 1.7$), based on fits to the galaxy disc profiles in Leroy et al. (2008). This number is in good agreement with typical ratios of 1.5–2.0 between H I and optical disk sizes (Verheijen & Sancisi 2001). Kravtsov (2013) finds a $\chi_{\rm gas} = 2.6$, when normalizing gas profiles to a radius r_n obtained using abundance matching arguments.

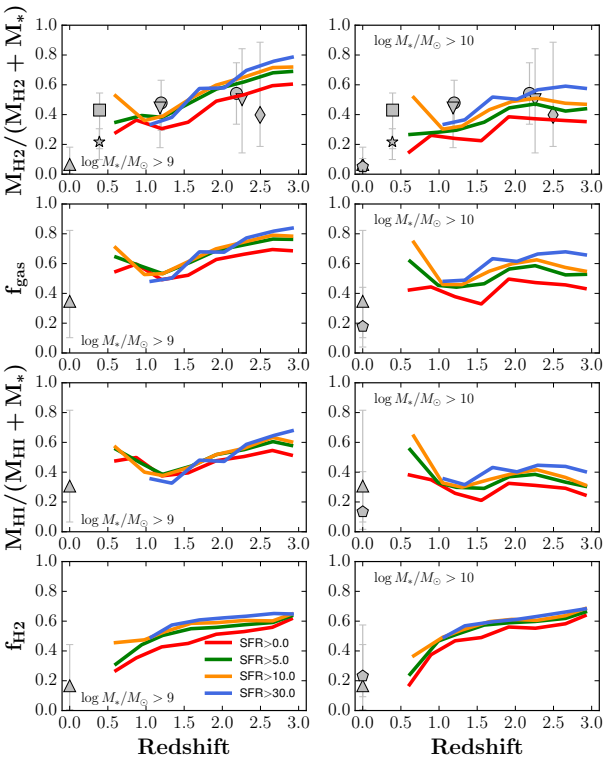

Figure 18. Redshift evolution of the relative H_2 content $\frac{M_{H2}}{M_{H2}+M_*}$ (top row), gas fraction (second row), relative H I content (third row), and molecular hydrogen fraction (bottom row) for galaxies with stellar masses in the range $M_* > 10^9\,M_\odot$ (left panels), $M_* > 10^{10}\,M_\odot$ (right panels), and SFR larger than 0 (red), 5 (green), 10 (orange), and 30 (blue) $M_\odot\,yr^{-1}$. Different markers represent the following datasets: *upwards pointing triangles*: galaxies from the THINGS survey (Leroy et al. 2008) at $z = 0.0$, *pentagons*: galaxies from the COLD GASS survey (Saintonge et al. 2011) at $z = 0.0$, *squares*: galaxies from Bauermeister et al. (2013) at $z \sim 0.4$, *stars*: galaxies from Geach et al. (2011) at $z \sim 0.4$, *circles*: galaxies from the PHIBBS survey (Tacconi et al. 2013) at $z \sim 1.2$ and $z \sim 2.2$, *downwards pointing triangles*: galaxies at $z \sim 1.2$ and $z \sim 2.2$ from Tacconi et al. (2010), *diamonds*: galaxies at $z \sim 2.2$ from (Saintonge et al. 2013). Error bars show the 80 percent confidence interval for each observational sample at the given redshift bin.

Furthermore, the value for χ_{gas} may vary as a function of redshift or galaxy properties. Varying χ_{gas} results in negligible differences in inferred cold gas and H_2 mass as long as $\chi_{gas} > 1$. Decreasing χ_{gas} to values less than one leads to more significant differences in the inferred gas masses. When adopting the extreme case of $\chi_{gas} = 0.5$ we find that the inferred gas and molecular masses are lowered by 0.25 and 0.1 dex, respectively. Observations of the sizes of the CO discs at $z \sim 1.2$ and $z \sim 2.2$ (supposedly tracing the molecular hydrogen) do not support a scale length ratio of $\chi_{gas} < 1.0$ (e.g. Tacconi et al. 2010, 2013). Berry et al. (2014) found that in semi-analytic models H I discs have to be more extended than the stars in order to reproduce Damped Lyman-alpha properties (Schaye 2001).

A key ingredient in our model is the partitioning of cold gas into a molecular and atomic component using a pressure-based recipe presented in Blitz & Rosolowsky (2006). This recipe was calibrated based on observations in local galaxies (Blitz & Rosolowsky 2006; Leroy et al. 2008) and has not yet been constrained at our redshifts of interest. An increased UV background or lower gas metallicities could suppress the formation of molecules on dust grains and the ability of the molecular hydrogen to self-shield. Under these conditions our model would require a larger inferred cold gas reservoir to support the observed SFRs. We anticipate that future high-resolution observations with ALMA and SKA will be able to assess the validity of these locally calibrated relations at high redshifts. An alternative approach would be to use a molecular hydrogen prescription that is also a function of gas phase metallicity (e.g., Krumholz, McKee & Tumlinson 2009; Gnedin & Kravtsov 2011). Similarly to the pressure based algorithm, these prescriptions have also only been tested against local observations (e.g. Fumagalli, Krumholz & Hunt 2010). A significant downside of applying this approach is that gas-phase metallicities are only available for a limited number of galaxies at our redshifts of interest. A different approach could be to use the fundamental metallicity relation (Mannucci et al. 2009) to estimate the gas-phase metallicity of galaxies as a function of their SFR and stellar mass. We opted not to use this approach, as this will introduce an additional empirical step and source of uncertainty. Moreover, the calibration of gas phase metallicity measurements is highly uncertain.

We assume an adapted version of the SF relation presented in Bigiel et al. (2008) to allow for an increased star formation efficiency in high-surface-density environments. When not accounting for the increased star-formation efficiency (i.e. $N_{SF} = 0$), the presented method predicts larger values for the gas content of galaxies with $SFR/(2\pi r_*^2) \approx 1\,M_\odot yr^{-1}kpc^{-2}$ by roughly 10 percent and $SFR/(2\pi r_*^2) \approx 10\,M_\odot yr^{-1}kpc^{-2}$ by roughly 75 percent (less than 1 percent of our sample has a SFR surface density larger than $SFR/(2\pi r_*^2) \approx 10\,M_\odot yr^{-1}kpc^{-2}$).

To estimate the mid-plane pressure on the disc we adopt the prescription presented in Elmegreen (1989). We estimate the ratio between the gas and stellar vertical velocity dispersion following Fu et al. (2010), based on empirical scalings for nearby disc galaxies. Observations suggest that star-forming galaxies at $z \sim 2$ are "puffy" with high velocity dispersions (Förster Schreiber et al. 2009). Depending on the actual distributions of the giant molecular clouds and star-forming clumps, this may change the shielding properties of the molecular hydrogen.

An additional source of uncertainty lies in the conversion from CO emission to H_2 mass (see Bolatto, Wolfire & Leroy 2013, for a review) or the conversion from sub-mm dust continuum to gas mass. Our method is calibrated on H_2 masses that rely on the aforementioned conversions. Our method therefore includes these uncertainties.

In (e.g., Popping et al. 2012, , Figure 3) we showed that propagating the uncertainty in the input parameters (stellar mass, SFR, and size), the typical systematic uncertainty in inferred gas masses is approximately 0.3 dex. Many of the uncertainties cannot be well quantified. Combining all the concerns discussed above as well as the concerns discussed in Popping et al. (2012, Section 3.3), and taking the errors in the input parameters into account, we estimate an uncertainty in the inferred gas masses for our method is approximately 0.7 dex.

5 DISCUSSION

5.1 Galaxy gas fractions

The gas fraction of a galaxy is set by the competition between the inflow, outflow, and consumption of cold gas in the galaxy (Bouché et al. 2010; Davé, Finlator & Oppenheimer 2011; Dekel & Mandelker 2014). The cosmic SFR peaks at $z \sim 2$ (Hopkins & Beacom 2006; Madau & Dickinson 2014), and analytic calculations and cosmological hydrodynamical simulations predict large gas accretion rates onto galaxies at this epoch (Birnboim & Dekel 2003; Kereš et al. 2005, 2009; Dekel & Birnboim 2006; Dekel et al. 2009). Our indirect gas measures provide an ideal sample to constrain which of the aforementioned processes dominate this competition at different cosmic times. We find that gas fractions decrease most rapidly at $z < 1.5$, although a gradual decrease is present at all redshifts studied in this sample. These results suggest that the accretion of gas onto galaxies cannot keep up with the consumption and/or outflow of gas, especially at redshifts $z < 2$ (see also Popping et al. 2012). These results are in good qualitative agreement with predictions from semi-analytic and semi-empirical models (e.g., Obreschkow & Rawlings 2009; Lagos et al. 2011; Fu et al. 2012; Popping, Somerville & Trager 2014; Popping, Behroozi & Peeples 2015). Besides the relative gas content, the molecular fraction of the cold gas also decreases with time, most rapidly at $z < 2$ (Saintonge et al. 2013). The characteristic density of the cold gas decreases (Popping et al. 2014), allowing less gas to self-shield and become molecular. This indicates that the physical process that suppresses star-formation with time is at least two-fold: galaxies run out of gas as well as molecules, but not necessarily at the same rate. For the most massive galaxies in our sample this two-fold process is already taking place at $z \sim 3$, well before the peak in cosmic SFR and before the accretion of cold gas onto galaxies slows due to the increasing dominance of dark energy driven expansion. This is an important constraint for models of galaxy formation that include H_2-based star-formation recipes.

The rapid decrease in cold gas fractions below $z < 1.5$ is supported by direct observations of the CO emission in galaxies (Figure 18 Tacconi et al. 2013; Saintonge et al. 2013). These observations indicate that the relative H_2 content of galaxies remains flat above redshifts of $z \sim 2$ and gradually decreases at lower redshifts. The slope and normalization of this trend is in part set by the selection criteria. Depending on the selection criteria in stellar mass and SFR chosen, the evolution of $f_{\rm H2*}$ at redshifts $z > 2$ can change.

Popping et al. (2012) found for a sample of galaxies taken from COSMOS at redshifts $0.5 < z < 2$ that the cold gas fraction of galaxies with stellar masses of $\sim 10^{10.5}\,{\rm M}_\odot$ evolves from $f_{\rm gas} \sim 1$ at $1.75 < z < 2$ to $f_{\rm gas} \sim 0.2$ at $0.5 < z < 0.75$. The authors found that less-massive galaxies showed hardly any evolution in their gas fractions. This difference suggested that massive galaxies become gas-poor earlier and quicker than less massive galaxies; this behaviour was characterized as downsizing in gas content. Furthermore, the authors found a characteristic stellar mass below which the gas fraction of galaxies rapidly drops. This characteristic mass decreased towards lower redshifts. We find a similar characteristic stellar mass at redshift $2.5 < z < 3$, but the drop in the relation between cold gas mass and stellar mass disappears towards lower redshifts. Also, there is no strong difference in the rate at which the highest mass galaxies run out of cold gas compared to the least massive galaxies in our sample (see Figure 11). We remind the reader that the CANDELS survey allows us to study much fainter objects and is not biased towards the most star-forming objects. We ascribe the conclusion reached in Popping et al. (2012) to the selection of only the most actively star-forming, and therefore most gas rich, galaxies at stellar masses less than $10^{9.5}\,{\rm M}_\odot$. Our results suggests a gradual evolution in the cold gas fraction and the relative molecular hydrogen content of galaxies at $0.5 < z < 3$, independent of stellar mass.

5.2 Extended parameter space and selection effects

With the technique used in this work we can easily infer the cold gas masses for large samples of galaxies, covering a wide range in stellar mass, SFR, and redshift. As discussed above, this allows us to evaluate the impact of selection effects on smaller surveys of directly measured gas masses and to extend observed relations to stellar mass, SFR, and redshift regimes where gas measure are hard to obtain directly.

CO observations of actively star-forming galaxies have revealed a linear relation between H_2 mass and stellar mass (e.g. Saintonge et al. 2013; Tacconi et al. 2013). Our results suggest that this relation was already in place at $z = 3$, when the Universe was less than 3 Gyr old and extends down to stellar masses of at least $10^8\,{\rm M}_\odot$. A similar relation (although less well defined) is found for the total cold gas mass and H I mass. The trend between stellar mass and H I mass has larger scatter than the trend between stellar mass and cold gas mass and H_2 mass. Even though the uncertainties in the gas masses are significant, these extended scaling relations suggest that the balance between the consumption and in- and outflow of gas in galaxies is already at place for galaxies with low stellar masses.

In Figure 18 we explored the direct effect of changing selection criteria on the evolution of gas fractions in galaxies. We found no qualitative difference between different selection criteria. The fraction of gas, H I, and H_2 in galaxies decreases gradually from $z = 3$ to $z = 0.5$. The absolute values of the gas fractions change by a factor of a few when changing the selection criteria. We find that for a sample of galaxies with stellar masses more massive than $10^9\,{\rm M}_\odot$ the inferred cold gas, H I, and H_2 fractions of galaxies remain nearly identical when galaxies with a reasonable amount of SF are selected (SFRs of a few solar masses per year). Future surveys with a stellar mass limit of $10^9\,{\rm M}_\odot$ should be able to robustly constrain the evolution of the gas content of galaxies contributing most to the stellar mass budget and stellar growth in our Universe.

We found good agreement between direct observations of the H_2 mass of galaxies and our inferred H_2 masses for the galaxies with the highest SFR in our sample (with ${\rm SFR} > 20 - 30\,{\rm M}_\odot\,{\rm yr}^{-1}$). Our results indicate that at the stellar masses probed by direct surveys, there is also a substantial population of galaxies with H_2 masses less massive than $10^{10}\,{\rm M}_\odot$. This group of galaxies should be accounted for when trying to make more generalized statements, especially when focusing on galaxies with large stellar masses.

5.3 A constant relation between H I mass and stellar mass

We found hardly any evolution in the relation between H I mass and stellar mass, whereas the relation between cold gas mass and H_2 mass with stellar mass does evolve. Popping, Behroozi & Peeples (2015) found a similar result when coupling an abundance matching model with the semi-empirical approach to infer gas masses adopted in this work. Semi-analytic, semi-empirical, and hydrodynamic models have also found a constant relation between H I mass and stellar mass remains constant with time (for galaxies with stellar masses larger than 10^9 $M_\odot$), just as the H I mass function out to $z = 2$ (Dutton, van den Bosch & Dekel 2010; Lagos et al. 2011; Fu et al. 2012; Davé et al. 2013; Popping, Somerville & Trager 2014; Popping, Behroozi & Peeples 2015).

Although already predicted by different models, this is the first time a model used actual observations as input to find a constant H I-to-stellar mass ratio. The relatively weak evolution in H I mass is driven by an apparent self-regulation that naturally arises in galaxies. As gas is consumed over time and galaxies grow as a function of stellar mass, the cold gas surface density decreases which naturally causes the H I fraction of the cold gas to increase. Although this process may prevent a rapid drop in the H I reservoirs of galaxies, by no means does this process imply that the H I mass at a fixed stellar mass should remain constant. There is a fine balance between the amount of cold gas being consumed, heated and/or expelled, and the partitioning of the remaining gas into an atomic and molecular component that sets the constant H I mass.

We are aware that this result should be placed within the context of the model framework adopted in this (and other) work. If the adopted recipes for SF and the partitioning of cold gas are not valid for galaxies at $z > 0$ this could also dramatically change our conclusions. We therefore look forward to surveys with the SKA pathfinders probing the H I mass of galaxies out to at least $z = 1$. If indeed the H I-to-stellar mass fraction of galaxies remains constant, it should be feasible to observe the H I mass of M_* galaxies at $z = 1$–1.5 (Carilli & Rawlings 2004).

5.4 Comparing predictions by a theoretical model to inferred gas masses

Semi-analytic models of galaxy formation start from a cosmological framework for structure formation, and include physical recipes to describe the baryonic physics acting on galaxies (such as the cooling and accretion of gas, star formation, and outflows). In this work we started from observed quantities and converted them into other quantities using empirical scaling laws. Although many of the ingredients are the same for the two approaches, their different nature makes them very complementary. Any tension between predictions from semi-analytic models and this work can shed light on the successes and failures of theoretical models.

We find that the Popping, Somerville & Trager (2014) semi-analytic model predicts three times less molecular hydrogen than our inferred gas masses suggest at redshifts $0.5 < z < 1.0$. The semi-analytic model predicts on average about 2 times less molecular hydrogen at redshifts $1.0 < z < 2.5$. The same holds for galaxies at redshifts $2.5 < z < 3$ with stellar masses less than 10^{10} $M_\odot$. Similarly, we find that the semi-analytic model predicts less cold gas in galaxies at redshifts $0.5 < z < 3$ than our inferred gas masses suggest.

Although the difference between semi-analytic model predictions and our inferred gas masses is not huge (and well within the uncertainty range of the method used in this work), it fits well within a broader picture where theoretical models predict too little SF for galaxies at redshifts $1 < z < 3$ (Somerville & Davé 2014). If the molecular hydrogen masses of modeled galaxies are too low for their stellar mass, the SFRs of those galaxies will be too low as well when a molecular gas based star-formation recipe is used.

Popping, Behroozi & Peeples (2015) extended the sub-halo abundance matching approach with recipes to infer cold gas masses. They found that the same semi-analytic model as used in this work predicts less *molecular hydrogen and cold gas* at redshifts $1 < z < 3$ than their extended sub-halo abundance approach suggests (see also Somerville & Davé 2014; White, Somerville & Ferguson 2015). A comparison with different semi-analytic models (Obreschkow & Rawlings 2009; Lagos et al. 2011) yielded the same results, making this a more general problem.

5.5 What drives the star-formation efficiency of galaxies

We have shown that, when using our model, the molecular fraction of the cold gas is a very important quantity that cannot be neglected. Despite large total cold gas masses, low molecular fractions can suppress the formation of stars and result in low SFE.[5] Indeed the SFEs of galaxies on the relation between SFR and stellar mass increases with stellar mass (Saintonge et al. 2013). However, our model implies that the physical state of the cold gas varies strongly as a function of stellar mass along the stellar mass–SFR relation.

To understand the origin of the varying molecular fractions and SFE, we have to look at the galaxy properties that enter our model. Within our model the cold-gas and molecular-gas contents of a galaxy are set by a combination of its SFR, stellar mass, and size. Most important is the combination of SFR and scale radius, which sets the SFR surface density distribution of the galaxy. Within our model, low SFR surface densities result in low H_2 surface densities. However, to ensure the pressure of the gaseous disc is high enough for the cold gas to collapse and form molecules, low H_2 surface densities require relatively large cold-gas surface densities. This argument can also be reversed: an increase in the scale radius of the gaseous disc lowers the surface density of the cold gas, naturally causing less H_2 to self-shield and transform into stars. We see this in the galaxies with low stellar masses and large discs in our sample. These are galaxies with the highest gas fractions, but their molecular fractions and star-formation efficiencies are very low.

An increase in galaxy scale radius also has a significant effect on the SFE of galaxies with high stellar masses

[5] We again emphasize that in this work the star-formation efficiency is defined as the ratio between SFR and total (H I + H_2) cold gas mass, rather than just the molecular hydrogen mass

($M_* > 10^{10}\,M_\odot$). At fixed stellar mass galaxies with compact discs have higher SFEs (and molecular fractions) than galaxies with more extended discs. The lower surface densities allow for a higher shielding rate of the molecular hydrogen. At fixed stellar mass the SFE of galaxies also increases with increasing SFR. The change in SFE cannot account for differences in SFR of a few orders of magnitude, but it can lower the SFR by a factor of a few. To first order it is the absolute amount of cold gas that largely controls the gas density and SFR of a galaxy. The distribution of gas into an extended disc can act as a secondary mechanism to suppress the formation of molecules and lower a galaxy's SFR.

In reality the formation of molecules does not solely depend on the surface density or midplane pressure of cold gas. Dust grains and metals are the primary catalysts and coolants of H_2 formation. Dust grains also shield the molecular hydrogen from H_2 dissociation by UV photons and photo-electric heating. The metallicity of the ISM is therefore an important extra component that controls the formation of molecules, especially in low-density environments. In addition to low densities, a low-metallicity environment therefore stimulates the build-up of large atomic gas reservoirs, preventing the cold gas from condensing and forming stars (Krumholz & Dekel 2012b; Berry et al. 2014; Popping, Somerville & Trager 2014; Somerville, Popping & Trager 2015). We have not included this effect in our model, but it would strengthen the role that low surface densities and the partitioning of cold gas into H I and H_2 plays in the formation of stars. Furthermore, we have not discussed the destruction of molecular hydrogen by radiation from an AGN.

6 SUMMARY & CONCLUSIONS

We applied a method to infer the total cold gas and molecular gas content of a deep sample of galaxies from the CANDELS survey covering a redshift range of $0.5 < z < 3$. All data results in this paper are available for download online.[6] Our main results are as follows:

- There is an increasing trend between the inferred cold gas, H I, and H_2 mass and the stellar masses of galaxies, which is already in place at $z = 3.0$ and extends down to stellar masses of $10^8\,M_\odot$. The slopes of these trends are different from the slope of the relation between SFR and stellar mass.
- There is no simple one-to-one mapping between inferred cold gas mass and molecular-hydrogen mass. Large gas reservoirs do not necessarily lead to large H_2 reservoirs. The molecular fractions of cold gas increase with increasing stellar mass and look-back time.
- The cold gas fraction (f_{gas}) and relative amount of molecular hydrogen in galaxies (f_{H2*}) decrease gradually with time at a relatively constant rate, independent of stellar mass.
- The mean fraction of atomic hydrogen ($M_{HI}/(M_* + M_{HI})$) in galaxies at fixed stellar mass stays remarkably constant with time over the entire redshift probed.
- There is a large population of low-stellar-mass galaxies that are dominated by atomic gas. Only a minor fraction of their total gas content is molecular and can form stars.
- The inferred SFE of galaxies increases along the relation between SFR and stellar mass. Although part of the same trend, the most-massive galaxies in our sample have SFEs more than twice as high as lower-mass galaxies. At fixed stellar mass the SFE and molecular fraction of the cold gas increase with galaxy compactness.
- The adopted approach can be tremendously helpful in understanding the impact of selection biases for much smaller samples of directly observed gas masses, as well as extending scaling relation between gas mass and other galaxy properties to ranges and redshift difficult to reach through direct observations.

[6] `http://www.eso.org/~gpopping/Gergo_Poppings_Homepage/Data.html`

ACKNOWLEDGMENTS

We thank the referee for a thorough report and very constructive comments that have improved the paper. GP thanks Romeel Davé, Marco Spaans, and the galaxy group at the Kapteyn Institute in Groningen for stimulating input for this paper. This work is based on observations taken by the CANDELS Multi-Cycle Treasury Program with the NASA/ESA HST, which is operated by the Association of Universities for Research in Astronomy, Inc., under NASA contract NAS5-26555. GP acknowledges NOVA (Nederlandse Onderzoekschool voor Astronomie) for funding.

References

Barro G. et al., 2014, ApJ, 791, 52
Bauermeister A. et al., 2013, ApJ, 768, 132
Bavouzet N., Dole H., Le Floc'h E., Caputi K. I., Lagache G., Kochanek C. S., 2008, A&A, 479, 83
Bell E. F. et al., 2005, ApJ, 625, 23
Berry M., Somerville R. S., Haas M. R., Gawiser E., Maller A., Popping G., Trager S. C., 2014, MNRAS, 441, 939
Bigiel F., Blitz L., 2012, ApJ, 756, 183
Bigiel F., Leroy A., Walter F., Brinks E., de Blok W. J. G., Madore B., Thornley M. D., 2008, AJ, 136, 2846
Bigiel F. et al., 2011, ApJ, 730, L13+
Birnboim Y., Dekel A., 2003, MNRAS, 345, 349
Blitz L., Rosolowsky E., 2006, ApJ, 650, 933
Bolatto A. D., Leroy A. K., Rosolowsky E., Walter F., Blitz L., 2008, ApJ, 686, 948
Bolatto A. D., Wolfire M., Leroy A. K., 2013, ARA&A, 51, 207
Boselli A., Cortese L., Boquien M., Boissier S., Catinella B., Lagos C., Saintonge A., 2014, A&A, 564, A66
Bothwell M. S. et al., 2014, MNRAS, 445, 2599
Bouché N. et al., 2010, ApJ, 718, 1001
Brennan R. et al., 2015, ArXiv e-prints 1501.06840
Bruzual G., 2007, in Astronomical Society of the Pacific Conference Series, Vol. 374, From Stars to Galaxies: Building the Pieces to Build Up the Universe, A. Vallenari, R. Tantalo, L. Portinari, & A. Moretti, ed., pp. 303–+
Bruzual G., Charlot S., 2003, MNRAS, 344, 1000

Calzetti D., Armus L., Bohlin R. C., Kinney A. L., Koornneef J., Storchi-Bergmann T., 2000, ApJ, 533, 682
Caputi K. I., 2013, ApJ, 768, 103
Carilli C. L., Rawlings S., 2004, New A Rev., 48, 979
Chabrier G., 2003, PASP, 115, 763
Christensen C., Quinn T., Governato F., Stilp A., Shen S., Wadsley J., 2012, MNRAS, 425, 3058
Cortese L., Catinella B., Boissier S., Boselli A., Heinis S., 2011, MNRAS, 415, 1797
Daddi E. et al., 2010, ApJ, 713, 686
Dahlen T. et al., 2013, ApJ, 775, 93
Davé R., Finlator K., Oppenheimer B. D., 2011, MNRAS, 416, 1354
Davé R., Katz N., Oppenheimer B. D., Kollmeier J. A., Weinberg D. H., 2013, MNRAS, 434, 2645
Dekel A., Birnboim Y., 2006, MNRAS, 368, 2
Dekel A. et al., 2009, Nature, 457, 451
Dekel A., Mandelker N., 2014, MNRAS, 444, 2071
Dutton A. A., van den Bosch F. C., Dekel A., 2010, MNRAS, 405, 1690
Elbaz D. et al., 2011, A&A, 533, A119
Elmegreen B. G., 1989, ApJ, 338, 178
Erb D. K., Steidel C. C., Shapley A. E., Pettini M., Reddy N. A., Adelberger K. L., 2006, ApJ, 646, 107
Fadda D. et al., 2010, ApJ, 719, 425
Förster Schreiber N. M. et al., 2009, ApJ, 706, 1364
Fu J., Guo Q., Kauffmann G., Krumholz M. R., 2010, MNRAS, 409, 515
Fu J., Kauffmann G., Li C., Guo Q., 2012, MNRAS, 424, 2701
Fumagalli M., Krumholz M. R., Hunt L. K., 2010, ApJ, 722, 919
Galametz A. et al., 2013, ApJS, 206, 10
Geach J. E., Smail I., Moran S. M., MacArthur L. A., Lagos C. d. P., Edge A. C., 2011, ApJ, 730, L19
Genzel R. et al., 2012, ApJ, 746, 69
—, 2010, MNRAS, 407, 2091
—, 2014, ArXiv e-prints
Giavalisco M. et al., 2004, ApJ, 600, L93
Gnedin N. Y., Kravtsov A. V., 2011, ApJ, 728, 88
Grogin N. A. et al., 2011, ApJS, 197, 35
Guo Y. et al., 2013, ApJS, 207, 24
Henriques B., White S., Thomas P., Angulo R., Guo Q., Lemson G., Springel V., Overzier R., 2014, ArXiv e-prints
Holwerda B. W., Blyth S.-L., Baker A. J., 2012, in IAU Symposium, Vol. 284, IAU Symposium, Tuffs R. J., Popescu C. C., eds., pp. 496–499
Hopkins A. M., Beacom J. F., 2006, ApJ, 651, 142
Huang S., Haynes M. P., Giovanelli R., Brinchmann J., 2012, ApJ, 756, 113
Karim A. et al., 2011, ApJ, 730, 61
Kauffmann G. et al., 2003, MNRAS, 341, 54
Kennicutt, Jr. R. C., 1998a, ARA&A, 36, 189
—, 1998b, ApJ, 498, 541
Kereš D., Katz N., Fardal M., Davé R., Weinberg D. H., 2009, MNRAS, 395, 160
Kereš D., Katz N., Weinberg D. H., Davé R., 2005, MNRAS, 363, 2
Koekemoer A. M. et al., 2011, ApJS, 197, 36
Komatsu E. et al., 2009, ApJS, 180, 330
Kravtsov A. V., 2013, ApJ, 764, L31
Krumholz M. R., Dekel A., 2012a, ApJ, 753, 16
—, 2012b, ApJ, 753, 16
Krumholz M. R., McKee C. F., Tumlinson J., 2009, ApJ, 693, 216
Kuhlen M., Krumholz M. R., Madau P., Smith B. D., Wise J., 2012, ApJ, 749, 36
Lagos C. D. P., Baugh C. M., Lacey C. G., Benson A. J., Kim H.-S., Power C., 2011, MNRAS, 1776
Lawrence A. et al., 2007, MNRAS, 379, 1599
Leroy A. K., Walter F., Brinks E., Bigiel F., de Blok W. J. G., Madore B., Thornley M. D., 2008, AJ, 136, 2782
Madau P., Dickinson M., 2014, ARA&A, 52, 415
Magdis G. E. et al., 2012, ApJ, 760, 6
Mannucci F. et al., 2009, MNRAS, 398, 1915
McKee C. F., Ostriker E. C., 2007, ARA&A, 45, 565
Noeske K. G. et al., 2007, ApJ, 660, L43
Obreschkow D., Rawlings S., 2009, MNRAS, 394, 1857
Pannella M. et al., 2009, ApJ, 698, L116
Popping G., Behroozi P. S., Peeples M. S., 2015, MNRAS, 449, 477
Popping G., Caputi K. I., Somerville R. S., Trager S. C., 2012, MNRAS, 425, 2386
Popping G., Pérez-Beaupuits J. P., Spaans M., Trager S. C., Somerville R. S., 2014, MNRAS, 444, 1301
Popping G., Somerville R. S., Trager S. C., 2014, MNRAS, 442, 2398
Saintonge A. et al., 2011, MNRAS, 415, 32
—, 2013, ArXiv e-prints: 1309.3281
—, 2012, ApJ, 758, 73
Santini P. et al., 2013, ArXiv e-prints: 1311.3670
Sargent M. T. et al., 2014, ApJ, 793, 19
Schaye J., 2001, ApJ, 559, 507
Schruba A. et al., 2011, AJ, 142, 37
Scoville N. et al., 2007, ApJS, 172, 1
—, 2014, ApJ, 783, 84
Solomon P. M., Rivolo A. R., Barrett J., Yahil A., 1987, ApJ, 319, 730
Somerville R. S., Davé R., 2014, ArXiv e-prints
Somerville R. S., Popping G., Trager S. C., 2015, ArXiv e-prints 1503.00755
Tacconi L. J. et al., 2010, Nature, 463, 781
—, 2013, ApJ, 768, 74
Troncoso P. et al., 2013, ArXiv e-prints: 1311.4576
Ueda Y. et al., 2008, ApJS, 179, 124
van der Wel A. et al., 2012, ApJS, 203, 24
—, 2014, ApJ, 788, 28
Verheijen M. A. W., Sancisi R., 2001, A&A, 370, 765
Wang J. et al., 2014, MNRAS, 441, 2159
Whitaker K. E. et al., 2014, ApJ, 795, 104
Whitaker K. E., van Dokkum P. G., Brammer G., Franx M., 2012, ApJ, 754, L29
White C. E., Somerville R. S., Ferguson H. C., 2015, ApJ, 799, 201
Wong T., Blitz L., 2002, ApJ, 569, 157
Wuyts S. et al., 2011, ApJ, 742, 96
Xue Y. Q. et al., 2011, ApJS, 195, 10